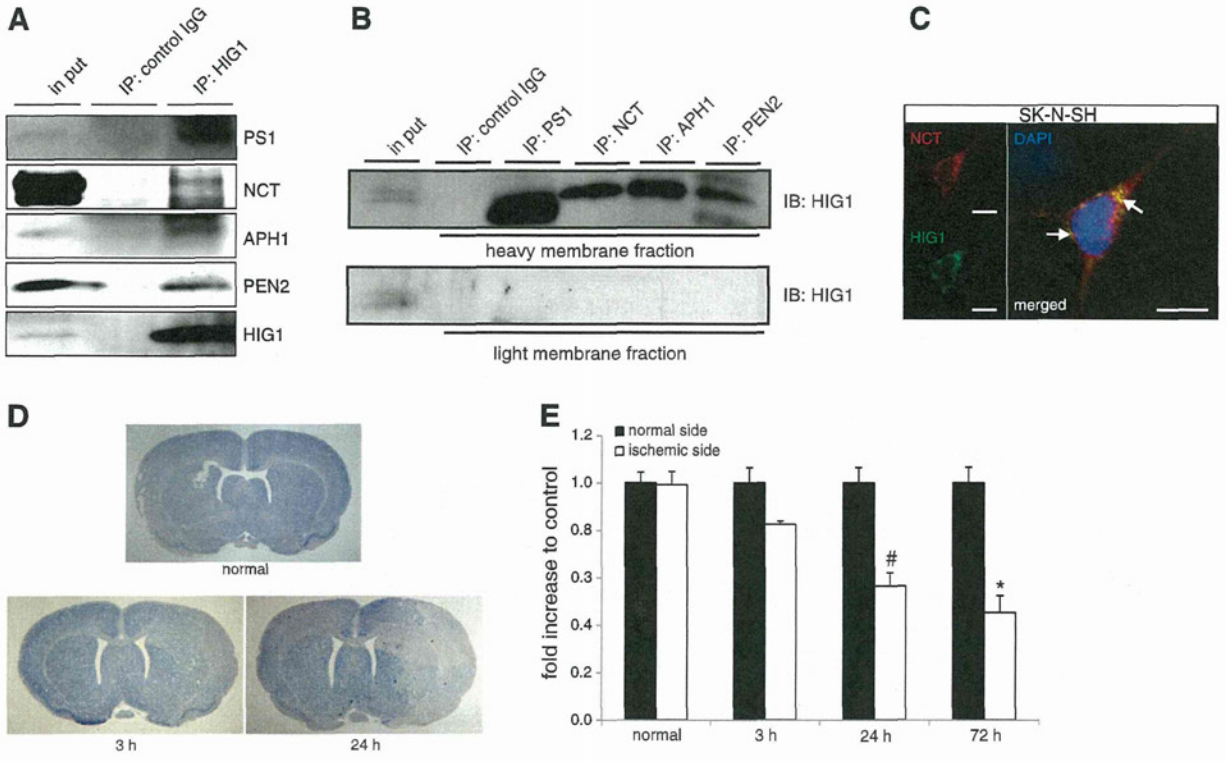

Figure 2. HIG1 was associated with the γ-secretase components and was down-regulated after rat MCAo model. *A*) γ-Secretase components (PS1, NCT, APH1, and PEN2) were coimmunoprecipitated with HIG1, followed by immunoblot in SK-N-SH. IP HIG1 indicates immunoprecipitation with the anti-HIG1 antibody. IP control IgG indicates immunoprecipitation with normal mouse IgG. *B*) HIG1 was coimmunoprecipitated with γ-secretase components, followed by immunoblot on heavy membrane fraction and light membrane fraction in SK-N-SH. *C*) Immunostaining analysis of endogenous HIG1 and γ-secretase component, NCT (×400 view). DAPI indicates nuclear staining (blue), HIG1 indicates staining with the anti-HIG1 antibody (green), and NCT indicates staining with the anti-nicastrin antibody (red). Scale bars = 10 μm. *D*) *In situ* hybridization of brain using HIG1 probe at 3 and 24 h after rat MCAo model. Right side is ischemic area. *E*) Quantitative real-time PCR of HIG1 expression level at 3, 24, and 72 h after rat MCAo model. β-Actin expression was used as a control expression. $^{\#}P < 0.005$, $^{*}P < 0.001$ *vs.* normal side.

HIG1 overexpression inhibits hypoxia-induced mitochondrial dysfunction

It is reported that increased γ-secretase activity and concentration of intracellular Aβ trigger mitochondrial dysfunction (12, 36). We evaluated whether HIG1 was involved in hypoxia-induced mitochondrial dysfunction. Interestingly, immunostaining analysis demonstrated that intracellular Aβ accumulated in the mitochondria under hypoxic conditions in control cells with APPswe overexpression, but not in cells that stably expressed HIG1 (72% decrease compared with control, $P<0.001$; **Fig. 4*A*, *B***). Next, we checked mitochondrial dysfunction by analyzing mitochondrial ROS production (Fig. 4*C*) and ATP production (Fig. 4*D*). Surprisingly, mitochondrial dysfunction was suppressed in cells that stably expressed HIG1. Moreover, in the analysis of mitochondrial ROS and ATP production, no additional effect of GSI on mitochondrial dysfunction in cells that overexpressed HIG1 was observed (Supplemental Fig. S4*A*, *B*). We checked mitochondrial condition in detail under hypoxia by using electron microscopy. Electron microscopic images demonstrated that many mitochondria were swollen due to the loss of cristae structure under hypoxic condition in control cells, but not in cells that stably expressed HIG1. Also, hypoxia-induced electron-dense deposits, which are thought to represent calcium deposits (37), were not observed in cells that stably expressed HIG1 (Fig. 4*E*). These results indicate that HIG1 has a suppressive role in hypoxia-induced mitochondrial dysfunction through the inhibition of γ-secretase activity.

Latter half of HIG1 is required for the interaction with γ-secretase and mitochondrial function

The predicted structure of HIG1 suggests that the protein possesses 2 transmembrane domains, as described previously (**Fig. 5*A***) (27). We designed two deletion constructs (deletion 1: 1–52 aa; deletion 2: 53–93 aa), including transmembrane domain 1 or 2, respectively, and investigated which part of HIG1 was required for its interaction with the γ-secretase complex using cells that stably expressed deletion mutants of HIG1 (Fig. 5*B*). Coimmunoprecipitation showed that deletion 2, but not deletion 1, was essential for association with the γ-secretase components (Fig. 5*C*). Although all HIG1 mutants were localized to the mitochondria (Fig. 5*D*), deletion 2, but not dele-

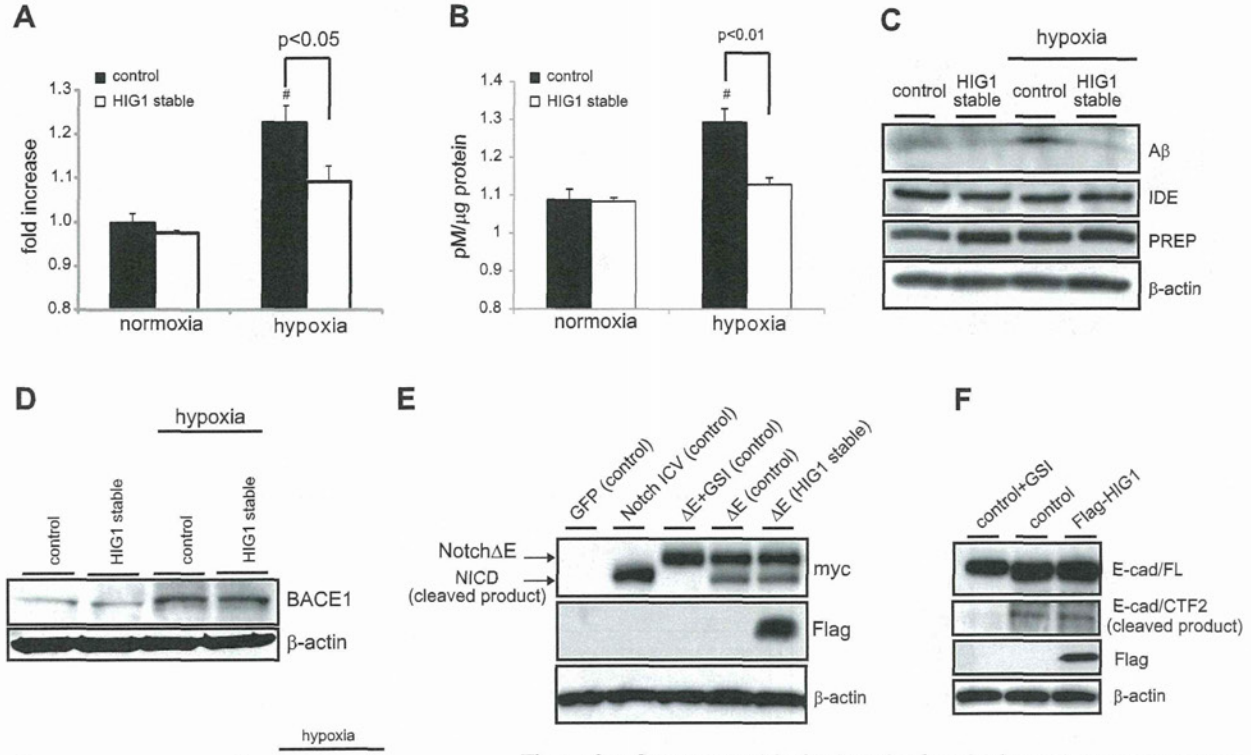

Figure 3. γ-Secretase activity in the mitochondrial membrane fraction and intracellular Aβ production were suppressed in cells that stably expressed HIG1. *A*) γ-Secretase activity in the mitochondrial fraction in control or HIG1 expressing cells under hypoxic conditions. Normoxia indicates no change in oxygen levels; hypoxia indicates treatment with reduced oxygen levels; $n = 5–8$. *B*) Intracellular Aβ40 production was measured by ELISA in APP-overexpressing control cells or HIG1-expressing cells after 24 h hypoxic conditions (control, 1.08±0.02; HIG1, 1.08±0.01; hypoxia+control, 1.29±0.03; hypoxia+HIG1, 1.12±0.01). $^{\#}P < 0.01$ *vs.* control; n=5–7. *C*) Western blot of control cells or cells that stably expressed HIG1 after overexpression of APP in the presence or absence of hypoxia. Aβ indicates anti-Aβ antibody; IDE indicates anti-IDE antibody; PREP indicates anti-PREP antibody; β-actin indicates anti-β-actin antibody, which was used as a loading control. *D*) Expression levels of APP processing enzyme, BACE1. No difference between APP-overexpressing control cells or HIG1-expressing cells was detected in expression levels of β-secretase, which produces C99 from APP, by Western blot in both normal condition and hypoxic condition (hypoxia). *E*) Analysis of Notch cleavage efficiency by γ-secretase in cells that stably expressed HIG1 (stable) and WT cells. ΔE indicates the membrane-anchored Notch derivative, which contains a γ-secretase cleavage site (NotchΔE). Intracellular variant (ICV) band indicates the γ-secretase cleavage product of ΔE (NICD). GSI, 10 μM L-685,458. β-Actin was used as a loading control. *F*) Efficacy of γ-secretase cleavage of E-cadherin (E-cad). E-cadherin full-length (FL) substrate and the E-cad/C-terminal fragment 2 (CTF2) products were analyzed by Western blot in HEK 293 cells. GSI, 10 μM L-685,458. β-Actin was used as a loading control. *G*) Expression of Flag-tagged HIG1 (Flag-HIG1) in APP-overexpressing control cells or HIG1-expressing cells. Cleaved product from full-length HIG1 was not observed by Western blot. β-Actin expression was used as a loading control.

tion 1, was required for the suppression of hypoxia-induced γ-secretase activity, assessed by an *in vitro* peptide cleavage assay (Fig. 5*E*). The suppression was accompanied by inhibition of hypoxia-induced ATP reduction (Fig. 5*F*). These results suggest that deletion 2 domain of HIG1 plays an important role in γ-secretase activity and mitochondrial function.

Mitochondrial γ-secretase activity and mitochondrial dysfunction are enhanced in HIG1-knockdown cells under hypoxic conditions

We evaluated the ability of endogenous HIG1 to regulate γ-secretase activity using miRNA knockdown, and the involvement of mitochondrial dysfunction. Although HIG1 knockdown did not affect the expression of the γ-secretase components, as compared to the control (**Fig. 6*A***), we found that γ-secretase activity was up-regulated in the mitochondrial fraction in HIG1-knockdown cells compared with control cells under both normoxic and hypoxic conditions (15% increase under normoxia, $P<0.005$ *vs.* control; 14% increase under hypoxia, $P<0.001$ *vs.* control; Fig. 6*B*). We checked mitochondrial function by ATP level and ROS production. Interestingly, ATP production was reduced after depletion of HIG1 compared with control cells under normoxic and hypoxic conditions (8% decrease

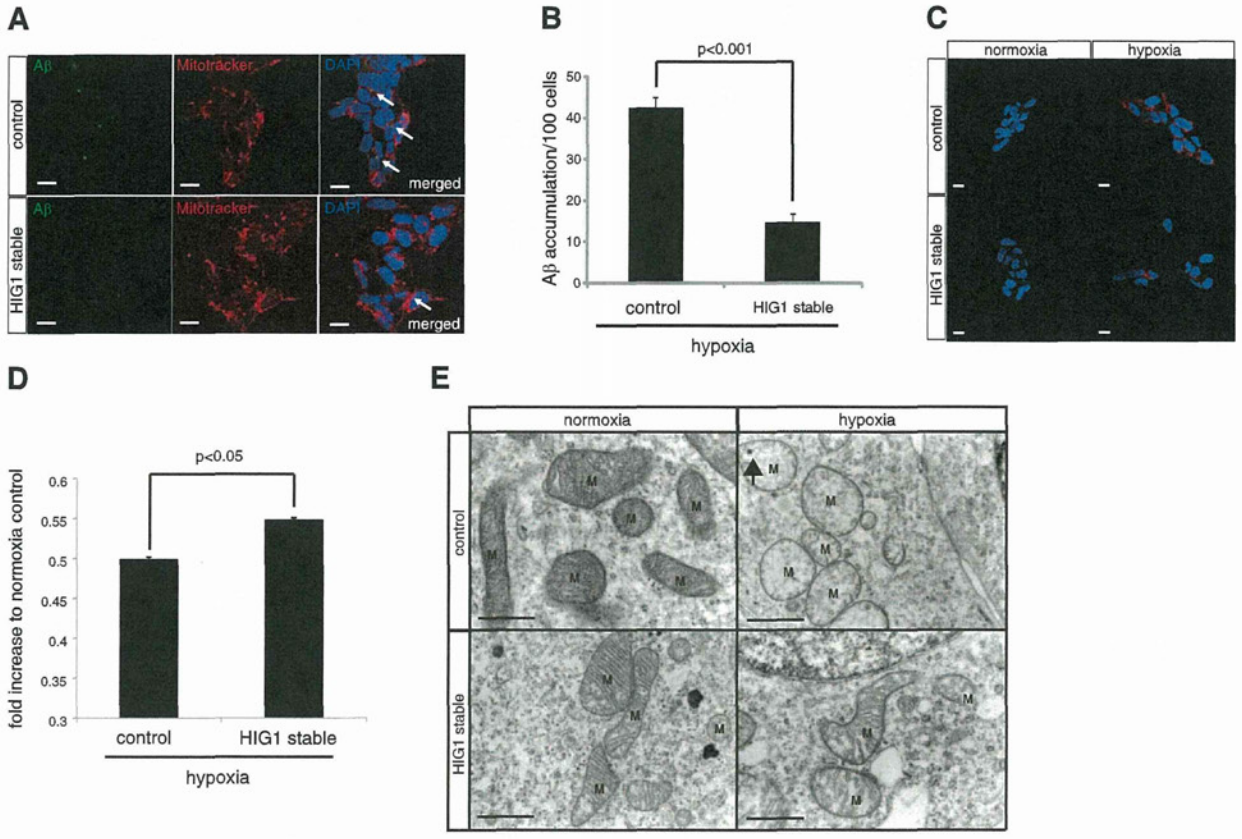

Figure 4. Mitochondrial Aβ accumulation and mitochondrial dysfunction were suppressed by overexpression of HIG1. *A*) Immunostaining analysis of Aβ in control cells or cells that stably expressed HIG1 after overexpression of APPswe under hypoxic conditions (×200 view). DAPI indicates nuclear staining (blue). Aβ indicates staining with the anti-Aβ antibody (green). Mitotracker indicates mitochondrial staining with 100 nM Mitotracker (red). *B*) Quantification of Aβ accumulation in the mitochondria. *C*) ROS production in control cells or cells stably expressing HIG1 under hypoxic conditions. ROS production from mitochondria was visualized with the fluorescence probe, mitoSOX (red), in control cells or cells stably expressing HIG1 under hypoxic conditions. Blue indicates nuclear staining. *D*) ATP generation in control cells or cells stably expressing HIG1 under hypoxic conditions. Each experiment was repeated ≥3 times. Control, 0.498 ± 0.003; HIG1, 0.548 ± 0.002; $P < 0.001$; $n = 5$–7. *E*) Representative electron microscopy images in SK-N-SH cells under hypoxic conditions. M, mitochondria. Arrow indicates an electron-dense deposit. Scale bars = 10 μm (*A*, *C*); 1 μm (*E*).

under normoxia, 8% decrease under hypoxia, $P<0.05$ *vs.* control; Fig. 6*C*). Moreover, mitochondrial ROS production in HIG1 knockdown cells was detected under normoxic conditions and was enhanced under hypoxic conditions (Fig. 6*D*). These results indicated that up-regulation of γ-secretase activity in mitochondria as a consequence of reduced HIG1 leads to mitochondrial dysfunction. We confirmed that knocking down or overexpressing HIG1 does not change the γ-secretase localization in the heavy membrane fraction (Supplemental Fig. S4*C*). Taken together, this study supported the possibility that HIG1 plays an important role in the maintenance of mitochondrial function *via* regulation of γ-secretase activity.

DISCUSSION

In this study, we showed that HIG1 plays an important role in the maintenance of mitochondrial function through its regulation of mitochondrial γ-secretase activity. Our results indicate that hypoxic conditions promote intracellular Aβ production and accumulation in the mitochondria of neuronal cells, but not in neuronal cells that stably express HIG1. This accumulation is thought to enhance ROS production and mitochondrial dysfunction, which leads to cell death. Aβ is known to localize to the mitochondria (36) and to induce mitochondrial toxicity (38, 39). There are several possible mechanisms for Aβ-induced mitochondrial toxicity. The accumulating Aβ could interact with mitochondrial enzyme, amyloid β binding alcohol dehydrogenase (ABAD) and inhibits glycolysis, the Krebs cycle and/or the respiratory chain pathways *via* increases in the concentrations of deleterious intermediate metabolites, which leads to ROS production (39, 40). In addition to metabolic inhibition by intracellular Aβ, it was reported recently that the interaction of Aβ with cyclophilin D (CypD) promotes ROS generation and the opening of mitochondrial permeability transition pores (mPTPs). The formation of mPTPs plays a key role in regulating mitochondrial-induced cell death

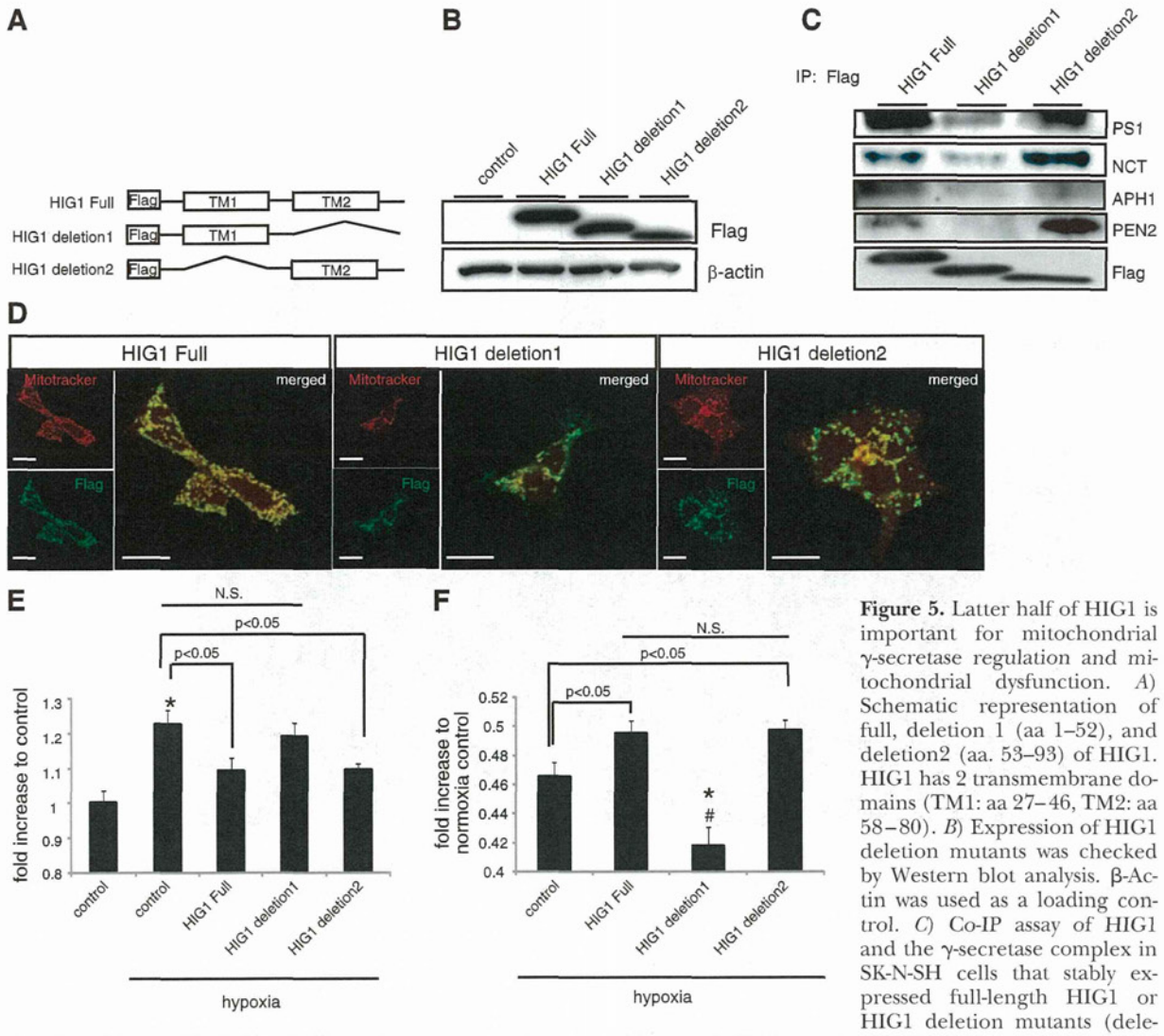

Figure 5. Latter half of HIG1 is important for mitochondrial γ-secretase regulation and mitochondrial dysfunction. *A*) Schematic representation of full, deletion 1 (aa 1–52), and deletion2 (aa. 53–93) of HIG1. HIG1 has 2 transmembrane domains (TM1: aa 27–46, TM2: aa 58–80). *B*) Expression of HIG1 deletion mutants was checked by Western blot analysis. β-Actin was used as a loading control. *C*) Co-IP assay of HIG1 and the γ-secretase complex in SK-N-SH cells that stably expressed full-length HIG1 or HIG1 deletion mutants (deletion 1 or deletion 2). IP Flag indicates immunoprecipitation with the anti-M2 Flag antibody. *D*) Representative confocal images after staining mitochondria (red, Mitotracker) and HIG1 deletion mutants (green, Flag) in HEK 293. Yellow in merged images indicates colocalization of mitochondria and HIG1-deletion mutants (×400 view). Scale bars = 20 μm. *E*) γ-Secretase activity in the mitochondrial fractions of control cells or cells that stably expressed full-length HIG1 or HIG1-deletion mutants under hypoxic conditions. $*P < 0.001$; $n = 6–8$. *F*) ATP content in control cells or cells stably expressing full-length or deletion mutants of HIG1 under hypoxic conditions (control, 0.465±0.010; HIG1 full, 0.494±0.009; HIG1 deletion 1, 0.417±0.013; HIG1 deletion 2, 0.497±0.007). $\#P < 0.001$ *vs.* hypoxia control; $*P < 0.005$ *vs.* hypoxia HIG1 full; $n = 6–8$. Each experiment repeated ≥3 times. Hypoxia indicates treatment with hypoxia for 24 h; N.S., not significant.

(38). These results indicate that intracellular and mitochondrial Aβ accumulation eventually leads to cell death through mitochondrial dysfunction; thus, inhibition of intracellular Aβ production might be a key target for the treatment of Alzheimer's disease and ischemic disorders.

Our results suggest that HIG1 is not only a novel regulator of γ-secretase on the mitochondrial membrane, but also important for mitochondrial function, including ROS production. Indeed, HIG1-knockdown experiments showed that depletion of HIG1 enhanced ROS production, even under normoxic conditions. The critical function of mitochondria is to produce ATP and act as the energy generators in the cell. They are especially vital in the brain and heart tissues, where high concentrations of ATP are required; however, a high level of ROS is produced as a by-product of high ATP production. In these organs, the levels of ROS production are relatively high (41). Recently, it was reported that oxidative stress is linked to aging and related diseases in fission yeast (42). Surprisingly, the expression level of HIG1 is very high in the brain and heart compared with other organs (Supplemental Fig. S1*A*). This suggests that HIG1 might suppress excessive ROS production in these organs and protect them from oxidative stress. In addition, under hypoxic conditions, γ-secretase activity was markedly increased; however, we found that HIG1 expression was not rapidly increased

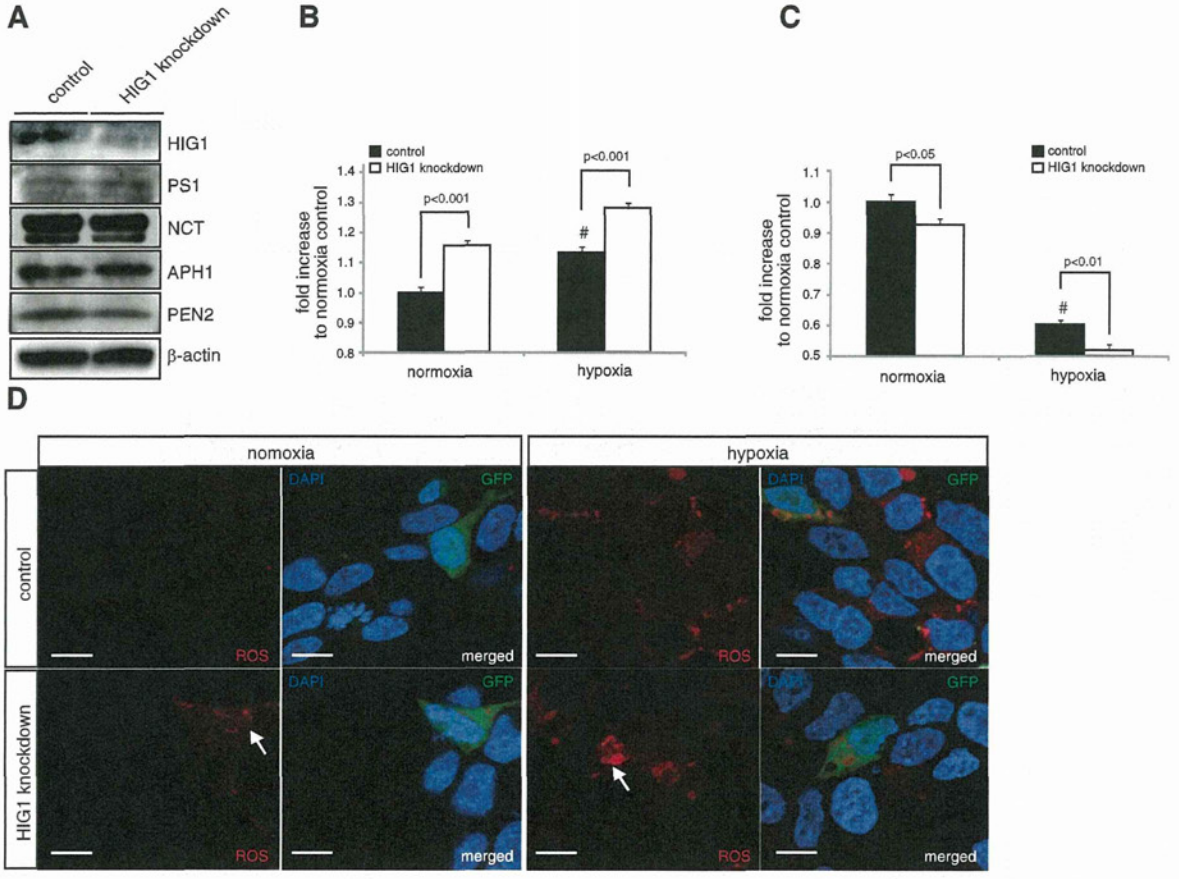

Figure 6. HIG1 knockdown enhanced hypoxia-induced γ-secretase activity and mitochondrial dysfunction. Expression of HIG1 and γ-secretase components (PS1, NCT, APH1, and PEN2) was analyzed by Western blot after HIG1 knockdown by miRNA. β-Actin was used as a loading control. *B*) γ-Secretase activity in the mitochondrial fractions of control cells or cells treated with HIG1 miRNA. $^{\#}P < 0.001$ *vs.* normoxia control; $n = 5–7$. *C*) ATP generation in control cells or cells with HIG1 knocked down. Control indicates transfection with control miRNA; HIG1 knockdown indicates transfection with HIG1 miRNA 863 (control, 1.00±0.02; HIG1 knockdown, 0.92±0.02; hypoxia control, 0.60±0.01; hypoxia HIG1 knockdown, 0.52±0.02.) $^{\#}P < 0.001$ *vs.* normoxia control; $n = 6–8$. Each experiment was repeated ≥3 times. *D*) Representative images of mitochondrial ROS staining in SK-N-SH cells or in SK-N-SH cells that stably expressed HIG1. DAPI indicates nuclear staining (blue); GFP indicates cells transfected with miRNA (green, HIG1-knockdown cell; ×400 view). Arrows indicate enhancement of ROS production in HIG1-knockdown cells. Scale bars =10 μm.

in culture cells with hypoxic conditions (Supplemental Fig. S2*B*), and, unexpectedly, HIG1 mRNA expression was decreased at 24 or 72 h after cerebral infarction of rats (MCAo model) by *in situ* hybridization and real-time PCR (Fig. 2*D*, *E*). On the basis of these results, HIG1 can be involved in maintenance of mitochondrial function and the mismatch between HIG1 and γ-secretase activity under hypoxic condition may lead to excess Aβ accumulation, which leads to mitochondrial dysfunction.

Currently, therapies involving γ-secretase inhibition have been pursued at the plasma membrane level, because the activity of γ-secretase on the plasma membrane was thought to be important for the progression of Alzheimer's disease. However, for clinical applications of GSIs, their influence on other substrates of γ-secretase, most importantly Notch, must be considered due to potential side effects, such as carcinogenesis (43, 44). In a recent study, inhibition of γ-secretase activity by a GSI suppressed mitochondrial dysfunction, including ROS production in neuronal cells that stably expressed APPswe, which, possibly, led to a reduction in cell death (12). On the basis of our results, HIG1 could suppress mitochondrial γ-secretase activity without affecting Notch cleavage, and protect the cell from mitochondrial dysfunction. These results demonstrated for the first time that γ-secretase activity at the mitochondrial membrane, but not at the plasma membrane, might be directly involved in mitochondrial dysfunction under pathological conditions. HIG1, a novel γ-secretase regulator at the mitochondrial membrane, might be an ideal and effective therapeutic target for Alzheimer's disease with minimal side effects; however, further experiments are required to investigate any indirect effects of HIG1 on mitochondrial function that are not involved in γ-secretase regulation. In summary, we identified HIG1 as a γ-secretase inhibitor in the mitochondria and its role in regulating mitochondrial function. FJ

The authors thank Prof. Noriaki Mitsuda (Ehime University, Ehime, Japan) for providing the human neuroblastoma cell line, SK-N-SH. pCS2+Notch1 ICV 6mt (6 myc-tagged Notch1 intracellular domain) and pCS2+Notch1 ΔETM 6mt (6 myc-tagged Notch1 extracellular transmembrane domain) were kind gifts from Dr. Raphael Kopan (Washington University, St. Louis, MO, USA). This work was supported, in part, by the Japan Society for the Promotion of Science.

REFERENCES

1. Haass, C., and Selkoe, D. J. (1993) Cellular processing of beta-amyloid precursor protein and the genesis of amyloid beta-peptide. *Cell* **75,** 1039–1042
2. Arumugam, T. V., Chan, S. L., Jo, D. G., Yilmaz, G., Tang, S. C., Cheng, A., Gleichmann, M., Okun, E., Dixit, V. D., Chigurupati, S., Mughal, M. R., Ouyang, X., Miele, L., Magnus, T., Poosala, S., Granger, D. N., and Mattson, M. P. (2006) Gamma secretase-mediated Notch signaling worsens brain damage and functional outcome in ischemic stroke. *Nat. Med.* **12,** 621–623
3. Aoyama, T., Takeshita, K., Kikuchi, R., Yamamoto, K., Cheng, X. W., Liao, J. K., and Murohara, T. (2009) gamma-Secretase inhibitor reduces diet-induced atherosclerosis in apolipoprotein E-deficient mice. *Biochem. Biophys. Res. Commun.* **383,** 216–221
4. Shih Ie, M., and Wang, T. L. (2007) Notch signaling, gamma-secretase inhibitors, and cancer therapy. *Cancer Res.* **67,** 1879–1882
5. De Strooper, B. (2003) Aph-1, Pen-2, and Nicastrin with Presenilin generate an active gamma-secretase complex. *Neuron* **38,** 9–12
6. Kimberly, W. T., LaVoie, M. J., Ostaszewski, B. L., Ye, W., Wolfe, M. S., and Selkoe, D. J. (2003) Gamma-secretase is a membrane protein complex comprised of presenilin, nicastrin, Aph-1, and Pen-2. *Proc. Natl. Acad. Sci. U. S. A.* **100,** 6382–6387
7. Evin, G., Canterford, L. D., Hoke, D. E., Sharples, R. A., Culvenor, J. G., and Masters, C. L. (2005) Transition-state analogue gamma-secretase inhibitors stabilize a 900 kDa presenilin/nicastrin complex. *Biochemistry* **44,** 4332–4341
8. Gu, Y., Sanjo, N., Chen, F., Hasegawa, H., Petit, A., Ruan, X., Li, W., Shier, C., Kawarai, T., Schmitt-Ulms, G., Westaway, D., St George-Hyslop, P., and Fraser, P. E. (2004) The presenilin proteins are components of multiple membrane-bound complexes that have different biological activities. *J. Biol. Chem.* **279,** 31329–31336
9. Zhou, S., Zhou, H., Walian, P. J., and Jap, B. K. (2005) CD147 is a regulatory subunit of the gamma-secretase complex in Alzheimer's disease amyloid beta-peptide production. *Proc. Natl. Acad. Sci. U. S. A.* **102,** 7499–7504
10. Chen, F., Hasegawa, H., Schmitt-Ulms, G., Kawarai, T., Bohm, C., Katayama, T., Gu, Y., Sanjo, N., Glista, M., Rogaeva, E., Wakutani, Y., Pardossi-Piquard, R., Ruan, X., Tandon, A., Checler, F., Marambaud, P., Hansen, K., Westaway, D., St George-Hyslop, P., and Fraser, P. (2006) TMP21 is a presenilin complex component that modulates gamma-secretase but not epsilon-secretase activity. *Nature* **440,** 1208–1212
11. Hansson, C. A., Frykman, S., Farmery, M. R., Tjernberg, L. O., Nilsberth, C., Pursglove, S. E., Ito, A., Winblad, B., Cowburn, R. F., Thyberg, J., and Ankarcrona, M. (2004) Nicastrin, presenilin, APH-1, and PEN-2 form active gamma-secretase complexes in mitochondria. *J. Biol. Chem.* **279,** 51654–51660
12. Sheng, B., Gong, K., Niu, Y., Liu, L., Yan, Y., Lu, G., Zhang, L., Hu, M., Zhao, N., Zhang, X., Tang, P., and Gong, Y. (2009) Inhibition of gamma-secretase activity reduces Abeta production, reduces oxidative stress, increases mitochondrial activity and leads to reduced vulnerability to apoptosis: implications for the treatment of Alzheimer's disease. *Free Radic. Biol. Med.* **46,** 1362–1375
13. Knott, A. B., Perkins, G., Schwarzenbacher, R., and Bossy-Wetzel, E. (2008) Mitochondrial fragmentation in neurodegeneration. *Nat. Rev. Neurosci.* **9,** 505–518
14. Zhang, J., Mori, A., Chen, Q., and Zhao, B. (2006) Fermented papaya preparation attenuates beta-amyloid precursor protein: beta-amyloid-mediated copper neurotoxicity in beta-amyloid precursor protein and beta-amyloid precursor protein Swedish mutation overexpressing SH-SY5Y cells. *Neuroscience* **143,** 63–72
15. Hayashi, H., Nakagami, H., Takami, Y., Sato, N., Saito, Y., Nishikawa, T., Mori, M., Koriyama, H., Tamai, K., Morishita, R., and Kaneda, Y. (2007) Involvement of gamma-secretase in postnatal angiogenesis. *Biochem. Biophys. Res. Commun.* **363,** 584–590
16. Meunier, C., Bordereaux, D., Porteu, F., Gisselbrecht, S., Chretien, S., and Courtois, G. (2002) Cloning and characterization of a family of proteins associated with Mpl. *J. Biol. Chem.* **277,** 9139–9147
17. Skovronsky, D. M., Doms, R. W., and Lee, V. M. (1998) Detection of a novel intraneuronal pool of insoluble amyloid beta protein that accumulates with time in culture. *J. Cell Biol.* **141,** 1031–1039
18. Hayashi, H., Nakagami, H., Takami, Y., Koriyama, H., Mori, M., Tamai, K., Sun, J., Nagao, K., Morishita, R., and Kaneda, Y. (2009) FHL-2 suppresses VEGF-induced phosphatidylinositol 3-kinase/Akt activation via interaction with sphingosine kinase-1. *Arterioscler. Thromb. Vasc. Biol.* **29,** 909–914
19. Shimamura, M., Sato, N., Sata, M., Kurinami, H., Takeuchi, D., Wakayama, K., Hayashi, T., Iida, H., and Morishita, R. (2007) Delayed postischemic treatment with fluvastatin improved cognitive impairment after stroke in rats. *Stroke* **38,** 3251–3258
20. Koibuchi, N., and Chin, M. T. (2007) CHF1/Hey2 plays a pivotal role in left ventricular maturation through suppression of ectopic atrial gene expression. *Circ. Res.* **100,** 850–855
21. Kim, S. K., Park, H. J., Hong, H. S., Baik, E. J., Jung, M. W., and Mook-Jung, I. (2006) ERK1/2 is an endogenous negative regulator of the gamma-secretase activity. *FASEB J.* **20,** 157–159
22. Senda, T., Nishii, Y., and Fujita, H. (1991) Immunocytochemical localization of synapsin I in the adrenal medulla of rats. *Histochemistry* **96,** 25–30
23. Nilsson, R., Ahmad, F., Sward, K., Andersson, U., Weston, M., Manganiello, V., and Degerman, E. (2006) Plasma membrane cyclic nucleotide phosphodiesterase 3B (PDE3B) is associated with caveolae in primary adipocytes. *Cell. Signal.* **18,** 1713–1721
24. Wieckowski, M. R., Giorgi, C., Lebiedzinska, M., Duszynski, J., and Pinton, P. (2009) Isolation of mitochondria-associated membranes and mitochondria from animal tissues and cells. *Nat. Protoc.* **4,** 1582–1590
25. Nishikawa, T., Nakagami, H., Matsuki, A., Maeda, A., Yo, C. Y., Harada, T., Morishita, R., Tamai, K., and Kaneda, Y. (2006) Development of high-throughput functional screening of therapeutic genes, using a hemagglutinating virus of Japan envelope vector. *Hum. Gene Ther.* **17,** 470–475
26. Tanahashi, H., and Yoshioka, K. (2008) RNA interference silencing of DRAL affects processing of amyloid precursor protein. *Neurosci. Lett.* **439,** 293–297
27. Wang, J., Cao, Y., Chen, Y., Chen, Y., Gardner, P., and Steiner, D. F. (2006) Pancreatic beta cells lack a low glucose and O_2-inducible mitochondrial protein that augments cell survival. *Proc. Natl. Acad. Sci. U. S. A.* **103,** 10636–10641
28. Anandatheerthavarada, H. K., Biswas, G., Robin, M. A., and Avadhani, N. G. (2003) Mitochondrial targeting and a novel transmembrane arrest of Alzheimer's amyloid precursor protein impairs mitochondrial function in neuronal cells. *J. Cell Biol.* **161,** 41–54
29. Wang, R., Zhang, Y. W., Zhang, X., Liu, R., Zhang, X., Hong, S., Xia, K., Xia, J., Zhang, Z., and Xu, H. (2006) Transcriptional regulation of APH-1A and increased gamma-secretase cleavage of APP and Notch by HIF-1 and hypoxia. *FASEB J.* **20,** 1275–1277
30. Shi, J., Yang, S. H., Stubley, L., Day, A. L., and Simpkins, J. W. (2000) Hypoperfusion induces overexpression of beta-amyloid precursor protein mRNA in a focal ischemic rodent model. *Brain Res.* **853,** 1–4
31. Jendroska, K., Hoffmann, O. M., and Patt, S. (1997) Amyloid beta peptide and precursor protein (APP) in mild and severe brain ischemia. *Ann. N. Y. Acad. Sci.* **826,** 401–405
32. Kienlen-Campard, P., Miolet, S., Tasiaux, B., and Octave, J. N. (2002) Intracellular amyloid-beta 1-42, but not extracellular soluble amyloid-beta peptides, induces neuronal apoptosis. *J. Biol. Chem.* **277,** 15666–15670
33. Leissring, M. A., Farris, W., Wu, X., Christodoulou, D. C., Haigis, M. C., Guarente, L., and Selkoe, D. J. (2004) Alternative translation initiation generates a novel isoform of insulin-

degrading enzyme targeted to mitochondria. *Biochem. J.* **383,** 439–446
34. Hwang, D. Y., Cho, J. S., Kim, C. K., Shim, S. B., Jee, S. W., Lee, S. H., Seo, S. J., Cho, J. Y., Lee, S. H., and Kim, Y. K. (2005) Aging-related correlation of insulin-degrading enzyme with gamma-secretase-generated products involving insulin and glucose levels in transgenic mice. *Neurochem. Res.* **30,** 1171–1177
35. Falkevall, A., Alikhani, N., Bhushan, S., Pavlov, P. F., Busch, K., Johnson, K. A., Eneqvist, T., Tjernberg, L., Ankarcrona, M., and Glaser, E. (2006) Degradation of the amyloid beta-protein by the novel mitochondrial peptidasome, PreP. *J. Biol. Chem.* **281,** 29096–29104
36. Manczak, M., Anekonda, T. S., Henson, E., Park, B. S., Quinn, J., and Reddy, P. H. (2006) Mitochondria are a direct site of A beta accumulation in Alzheimer's disease neurons: implications for free radical generation and oxidative damage in disease progression. *Hum. Mol. Genet.* **15,** 1437–1449
37. Solenski, N. J., diPierro, C. G., Trimmer, P. A., Kwan, A. L., and Helm, G. A. (2002) Ultrastructural changes of neuronal mitochondria after transient and permanent cerebral ischemia. *Stroke* **33,** 816–824
38. Du, H., Guo, L., Fang, F., Chen, D., Sosunov, A. A., McKhann, G. M., Yan, Y., Wang, C., Zhang, H., Molkentin, J. D., Gunn-Moore, F. J., Vonsattel, J. P., Arancio, O., Chen, J. X., and Yan, S. D. (2008) Cyclophilin D deficiency attenuates mitochondrial and neuronal perturbation and ameliorates learning and memory in Alzheimer's disease. *Nat. Med.* **14,** 1097–1105
39. Lustbader, J. W., Cirilli, M., Lin, C., Xu, H. W., Takuma, K., Wang, N., Caspersen, C., Chen, X., Pollak, S., Chaney, M., Trinchese, F., Liu, S., Gunn-Moore, F., Lue, L. F., Walker, D. G., Kuppusamy, P., Zewier, Z. L., Arancio, O., Stern, D., Yan, S. S., and Wu, H. (2004) ABAD directly links Abeta to mitochondrial toxicity in Alzheimer's disease. *Science* **304,** 448–452
40. Chen, X., and Yan, S. D. (2006) Mitochondrial Abeta: a potential cause of metabolic dysfunction in Alzheimer's disease. *IUBMB Life* **58,** 686–694
41. Mracek, T., Pecinova, A., Vrbacky, M., Drahota, Z., and Houstek, J. (2009) High efficiency of ROS production by glycerophosphate dehydrogenase in mammalian mitochondria. *Arch. Biochem. Biophys.* **481,** 30–36
42. Zuin, A., Gabrielli, N., Calvo, I. A., Garcia-Santamarina, S., Hoe, K. L., Kim, D. U., Park, H. O., Hayles, J., Ayte, J., and Hidalgo, E. (2008) Mitochondrial dysfunction increases oxidative stress and decreases chronological life span in fission yeast. *PLoS. One* **3,** e2842
43. Milano, J., McKay, J., Dagenais, C., Foster-Brown, L., Pognan, F., Gadient, R., Jacobs, R. T., Zacco, A., Greenberg, B., and Ciaccio, P. J. (2004) Modulation of notch processing by gamma-secretase inhibitors causes intestinal goblet cell metaplasia and induction of genes known to specify gut secretory lineage differentiation. *Toxicol. Sci.* **82,** 341–358
44. Wong, G. T., Manfra, D., Poulet, F. M., Zhang, Q., Josien, H., Bara, T., Engstrom, L., Pinzon-Ortiz, M., Fine, J. S., Lee, H. J., Zhang, L., Higgins, G. A., and Parker, E. M. (2004) Chronic treatment with the gamma-secretase inhibitor LY-411,575 inhibits beta-amyloid peptide production and alters lymphopoiesis and intestinal cell differentiation. *J. Biol. Chem.* **279,** 12876–12882

Received for publication September 9, 2011.
Accepted for publication February 7, 2012.

Published OnlineFirst December 18, 2012; DOI: 10.1158/1078-0432.CCR-12-1947

Clinical Cancer Research

Systemic Administration of a Novel Immune-Stimulatory Pseudovirion Suppresses Lung Metastatic Melanoma by Regionally Enhancing IFN-γ Production

Kotaro Saga, Katsuto Tamai, Takehiko Yamazaki, et al.

Clin Cancer Res 2013;19:668-679. Published OnlineFirst December 18, 2012.

Published OnlineFirst December 18, 2012; DOI: 10.1158/1078-0432.CCR-12-1947

Cancer Therapy: Preclinical

Clinical Cancer Research

Systemic Administration of a Novel Immune-Stimulatory Pseudovirion Suppresses Lung Metastatic Melanoma by Regionally Enhancing IFN-γ Production

Kotaro Saga, Katsuto Tamai, Takehiko Yamazaki, and Yasufumi Kaneda

Abstract

Purpose: Cancer immunotherapy has encountered many difficulties in the face of the expectation to eradicate cancer, and new breakthroughs are required. We have previously shown that UV-inactivated Sendai virus particles (hemagglutinating virus of Japan envelope; HVJ-E) induce immunity against multiple tumor types. In this study, a novel pseudovirion that stimulates more robust antitumor immunity was designed for cancer treatment.

Experimental Design: First, we found that culturing murine splenocytes with HVJ-E in combination with interleukin (IL)-12 resulted in a remarkable increase in IFN-γ production compared with that observed in splenocytes cultured with IL-12 alone. The synergistic effects of HVJ-E and IL-12 on IFN-γ production were caused by viral F proteins independently of HVJ-E fusion activity and not by hemagglutination from hemagglutinin-neuraminidase (HN) proteins. We next constructed HN-depleted HVJ-E expressing the Fc region of immunoglobulin G (IgG) on the envelope and single-chain IL-12 containing the ZZ domain of protein A to produce an IL-12–conjugated HVJ-E particle without hemagglutinating activity.

Results: IL-12–conjugated HVJ-E dramatically enhanced the amount of IFN-γ produced by immune cells. Intratumoral injection of IL-12–conjugated HVJ-E eradicated murine melanomas more effectively than injection of wild-type HVJ-E through increased production of melanoma-specific CTLs. IL-12–conjugated HVJ-E preferentially accumulated in the lungs after systemic administration. When small metastatic melanoma foci were formed in the lungs, systemic administration of IL-12–conjugated HVJ-E significantly reduced the number of metastatic foci by inducing local production of IFN-γ in the lungs and generating large numbers of melanoma-specific CTLs.

Conclusion: IL-12–conjugated HVJ-E is a promising tool for the treatment of cancers, including lung metastasis. *Clin Cancer Res; 19(3); 668–79. ©2012 AACR.*

Introduction

Cancer tissues use several systems to induce immunotolerance, including the activation of $FoxP3^+CD4^+CD25^+$ regulatory T cells (Treg; ref. 1). Therefore, although many types of anticancer drugs have been developed, the cure for cancer remains elusive. In recent years, much attention has been paid to cancer immunotherapy because it may suppress tumor metastasis and recurrence by activating immune cells to target cancer cells. Recently, several cancer immunotherapy systems (Provenge, ipilimumab, and anti-PD1) were developed. Provenge induces the activation of effector lymphocytes specific for cancer cells, and ipilimumab (anti-CTLA4 antibody) and the anti-PD1 antibody inhibit the downregulation of effector lymphocyte activity; these systems have shown beneficial effects for the treatment of cancer (2–6). Therefore, more effective immunotherapy should result from the activation of cancer-targeting effector lymphocytes and the suppression of immunosuppressive factors (7–9).

The Sendai virus (hemagglutinating virus of Japan; HVJ) belongs to the paramyxovirus family and has a negative-sense, single-strand RNA genome (10, 11) and 2 membrane glycoproteins. One of the glycoproteins is hemagglutinin-neuraminidase (HN), which binds to cell surface receptors, and the other is fusion protein (F), which allows for membrane fusion after binding to the receptors (10, 11). We recently reported that UV-inactivated HVJ (HVJ-envelope; HVJ-E) suppresses murine colon carcinoma (CT26) tumors by activating CTLs and eradicates murine renal cancer by activating natural killer (NK) cells (12, 13). Several cytokines and chemokines, such as IFN-β, CXCL10, and interleukin (IL)-6, are produced by dendritic cells in tumor

Authors' Affiliation: Division of Gene Therapy Science, Graduate School of Medicine, Osaka University, Suita, Osaka, Japan

Note: Supplementary data for this article are available at Clinical Cancer Research Online (http://clincancerres.aacrjournals.org/).

Corresponding Author: Yasufumi Kaneda, Division of Gene Therapy Science, Osaka University Graduate School of Medicine, 2-2 Yamadaoka, Suita, Osaka 565-0871, Japan. Phone: 81-6-6879-3900; Fax: 81-6-6879-3909; E-mail: kaneday@gts.med.osaka-u.ac.jp

doi: 10.1158/1078-0432.CCR-12-1947

Published OnlineFirst December 18, 2012; DOI: 10.1158/1078-0432.CCR-12-1947

Translational Relevance

Sendai virus-envelope (HVJ-E) has been shown to induce immunity to multiple types of tumors, and clinical trials to test its safety and antitumor immunity are ongoing in Japan. However, HVJ-E is not able to stimulate the production of IFN-γ, which is important for antitumor immunity. Therefore, to develop a second generation HVJ-E with enhanced antitumor activity, we constructed interleukin (IL)-12–conjugated, hemagglutinin-neuraminidase (HN)–depleted HVJ-E (IL-12–HVJ-E). Although IL-12 has a robust antitumor effect, the systemic administration of IL-12 is prohibited by the critical side effects resulting from systemic elevation in IFN-γ levels. In contrast, IL-12–HVJ-E accumulated in the lung following intravenous administration, induced local IFN-γ expression without increasing the serum IFN-γ level, and significantly reduced metastatic melanoma in the lung. Thus, IL-12–HVJ-E is a promising tool to treat metastatic lung cancers as well as regional cancers.

tissues and are associated with the antitumor immunity induced by HVJ-E. IL-6 plays a major role in tumor elimination. The antitumor activity of HVJ-E is abrogated by the suppression of IL-6 signaling with anti-IL-6 receptor antibodies in mice bearing CT26 cell-derived tumors (12), and HVJ-E fails to eliminate tumors in IL-6 knockout mice. HVJ-E inhibits Treg-mediated immunosuppression by inducing IL-6 secretion by mature dendritic cells (12). IL-6 most likely inhibits Tregs through increased methylation of the enhancer region of FoxP3, a key transcription factor of Tregs (14, 15). The F protein, one of the HVJ envelope proteins, has been found to be necessary for Toll-like receptor (TLR)–independent IL-6 production in dendritic cells.

Clinical studies to examine the safety and efficacy of HVJ-E have been conducted in patients with melanomas and prostate cancers at Osaka University Hospital (Suita, Japan) since 2009. To achieve more effective cancer immunotherapy, HVJ-E needs to be improved in the following ways. First, the inability of HVJ-E to directly induce IFN-γ production by immune cells must be addressed. IFN-γ is an important factor for antitumor activities, including the activation of CTLs and NK cells (16), the induction of chemokines that mediate T-cell infiltration into the tumor (17, 18), and the upregulation of MHC class I expression in tumor cells (19, 20). Previous reports have shown the importance of IFN-γ in cancer immunotherapy (21), and several clinical trials have shown the positive effect of IFN-γ treatment in cancer therapy (22–25). Second, HVJ-E should be improved to enable systemic administration. The HVJ-E currently used cannot be systemically administered because the HN protein induces hemagglutination in the blood. In this study, we attempted to overcome these limitations by developing a high-performance HVJ-E for more robust cancer immunotherapy.

IL-12 is a heterodimeric cytokine that is composed of p40 and p35 subunits and exhibits antitumor activity by stimulating IFN-γ secretion and promoting Th1 differentiation (26, 27). It has also been reported that single-chain (sc) IL-12, which connects p40 and p35, maintains the bioactivity of IL-12 (28, 29). Although systemic administration of IL-12 suppresses tumor growth (30), severe side effects are induced by the high serum levels of IFN-γ (31, 32). Thus, systemic administration of IL-12 has not been used clinically. Considering the advantages and disadvantages of IL-12 for cancer therapy, we used a combination of IL-12 and HVJ-E to enhance the antitumor activity of HVJ-E.

In this report, we found that IL-12 and HVJ-E acted synergistically to enhance IFN-γ production in a fusion-independent manner. We then showed that combination treatment with HN-depleted HVJ-E and scIL-12 induced much higher levels of IFN-γ secretion from cultured splenocytes than treatment with scIL-12 alone and eradicated tumors more effectively than treatment with HVJ-E alone. Systemic administration of scIL-12–conjugated HN-depleted HVJ-E successfully reduced the number of pulmonary metastatic foci in murine melanomas by regionally enhancing IFN-γ production in the lungs without elevating the serum IFN-γ levels.

Materials and Methods

Virus

HVJ (VR-105 parainfluenza1 Sendai/52, Z strain) was purchased from the American Type Culture Collection (ATCC), amplified in the chorioallantoic fluid of 10- to 14-day-old chick eggs and purified using centrifugation, as previously described (12, 13).

Mice

Female C57BL/6N mice were purchased from Japan Clea and maintained in a temperature-controlled, pathogen-free room. All animals were handled according to the approved protocols and guidelines of the Animal Committee of Osaka University (Suita, Japan).

Cell culture

Monkey kidney cells (LLCMK2) and F10 melanoma cells were purchased from the ATCC, and Chinese hamster ovary cells (CHO-K1) were purchased from the European Collection of Cell Cultures. LLCMK2, CHO-K1, F10 melanoma cells, and murine splenocytes were maintained in minimum essential medium (Gibco-BRL), Ham's F-12 medium (F-12; MP Biomedicals), Dulbecco's modified Eagle's medium (Nacalai Tesque Inc.), and RPMI-1640 medium (Nacalai Tesque Inc.), respectively. All media were supplemented with 10% FBS (Biowest), 100 U/mL penicillin, and 0.1 mg/mL streptomycin (Penicillin–Streptomycin Mixed Solution, Nacalai Tesque Inc.). β-Mercaptoethanol (4 nL/mL) was added to the media for the culture of splenocytes.

Plasmids

To construct the HN deletion mutants, Fc-HN and full-length HN, *HN* cDNA, which was kindly provided by

Published OnlineFirst December 18, 2012; DOI: 10.1158/1078-0432.CCR-12-1947

H. Taira (Iwate University, Iwate, Japan), was used as a template for amplification. Several HN deletion mutants (*ecto-400aa-HN*, *ecto-300aa-HN*, *ecto-200aa-HN*, *ecto-100aa-HN*, and *ecto-0aa-HN*) were generated using PCR. The Fc (CH2–CH3) domain of murine *IgG2a* cDNA was amplified from murine B cell cDNA, and Fc-HN was generated by connecting Fc and ecto-100aa-HN.

Murine *IL-12 p40* and *p35* cDNAs were amplified from murine splenocyte cDNA, and *scIL-12* was generated by connecting *p40* with the 5′-terminus of *p35* without including the first 66 nucleotides (the signal peptide sequence) via a $(GGGGS)_3$ linker. ZZ domain cDNA was amplified from pEZZ18 (GE Healthcare UK Ltd.) and fused with an HA-tag sequence at the 5′-terminus (HA-ZZ) using PCR. *ZZ-scIL-12* and *scIL-12* were generated by introducing the HA-ZZ or HA-tag sequence into the downstream signal peptide sequence of the p40 region.

To construct expression plasmids for the recombinant proteins, the coding regions were introduced into the CAGIpuro Gateway vector.

Gene transfer

The recombinant HN (rHN) expression vector was transferred to LLCMK2 cells using Lipofectamine (Invitrogen) and Plus Reagent (Invitrogen) according to the manufacturer's instructions.

Stable transformation

To generate a stable transformant of Fc-HN, LLCMK2 cells were transfected with CAGIpuro/*Fc-HN* using electroporation. A stable transformant was isolated by adding puromycin (4 μg/mL) to the culture medium. To generate a stable transformant of scIL-12 and ZZ-scIL-12, CHO-K1 cells were transfected with CAGIpuro/*scIL-12* and *ZZ-scIL-12* using electroporation. The respective stable transformants were isolated by adding puromycin (27 μg/mL) to the culture medium.

Production of ZZ-scIL-12 and scIL-12

The culture supernatant of CHO-K1 cells stably expressing scIL-12 and ZZ-scIL-12 was passed through a filter (pore size, 1.2 μm), and protease inhibitor cocktail tablets (Roche) were added to inhibit protein degradation. ScIL-12 and ZZ-scIL-12 were purified from the supernatant with EZview Red Anti-HA Affinity Gel (Sigma).

Generation of wt-HVJ-E, ΔHN-HVJ-E, and Fc-HVJ-E

For wt-HVJ-E, the culture medium of HVJ-infected LLCMK2 cells was passed through a filter (pore size, 1.2 μm) and then centrifuged at 100,000 × *g* for 2 hours at 4°C to precipitate the wt-HVJ particles. wt-HVJ was inactivated by UV irradiation (99 mJ/cm^2).

For ΔHN-HVJ-E, LLCMK2 cells were transfected with 100 pmol/mL HN-siRNA using Lipofectamine and Plus Reagent. Twenty-four hours after the transfection, the cells were infected with HVJ (1.5 particles/cell) for 1 hour. ΔHN-HVJ-E was collected using the same protocol as wt-HVJ-E.

Fc-HVJ-E was collected from LLCMK2 cells stably expressing Fc-HN using the same protocol as ΔHN-HVJ-E.

Generation of F_1/F_2-formed wt-HVJ-E and F-degraded ΔHN-HVJ-E

F_1/F_2-formed wt-HVJ-E was prepared by treating wt-HVJ-E with 5 μg/mL trypsin (Nacalai Tesque Inc.) for 30 minutes at 37°C. F-degraded ΔHN-HVJ-E was prepared by treating ΔHN-HVJ-E with 2.5 mg/mL trypsin for 24 hours at 37°C.

Production of scIL-12–HVJ-E

Fc-HVJ-E was treated with Factor Xa (5 μg/mL) for 2.5 hours at 23°C to activate the F protein, and then ZZ-scIL-12 (10 μg) was added. The mixture was placed in a 30% sucrose liquid solution (1.2 mL in a 1.5-mL tube) and centrifuged at 20,000 × *g* for 1 hour at 4°C. The pellets of scIL-12–HVJ-E were resuspended in PBS.

Sucrose density gradient centrifugation

A 25% to 50% sucrose gradient was created using the Gradient Master system (Towa Kagaku). A mixture of ZZ-scIL-12 and Fc-HVJ-E was placed in the sucrose gradient and centrifuged at 100,000 × *g* for 11 hours at 4°C.

Coprecipitation of Fc-HN with protein A-Sepharose

LLCMK2 cells transiently expressing Fc-HN and ecto-100aa-HN were solubilized with radioimmunoprecipitation assay (RIPA) buffer and protease inhibitor tablets, and the supernatant was mixed with protein A-Sepharose (GE Healthcare). The mixture was then centrifuged at 2,300 × *g* for 5 minutes at 4°C, and the protein that coprecipitated with protein A-Sepharose was solubilized with sample buffer for SDS-PAGE.

Western blot analysis

The samples were subjected to SDS-PAGE on 12% gels, and the proteins were transferred to Immobilon-P Transfer Membranes (Millipore Co.). To detect proteins, anti-HN (Scrum Inc.), anti-F (Scrum Inc.), anti-M (Hokkaido System Science Co., Ltd.), anti-Myc tag (Medical & Biological Laboratories Co., Ltd.), anti-HA tag (Sigma), or anti-β-actin (Sigma) immunoglobulin G (IgG) were used as primary antibodies. ECL horseradish peroxidase–conjugated donkey anti-rabbit IgG (GE Healthcare UK, Ltd.) was used as a secondary antibody for HN, F, and M detection, and ECL horseradish peroxidase–conjugated sheep anti-mouse IgG (GE Healthcare UK, Ltd.) was used as a secondary antibody for Myc tag, HA tag, and β-actin detection. ECL Western Blotting Detection Reagent (GE Healthcare UK, Ltd.) was used to detect the signals for each protein.

Immunostaining

rHN-transfected LLCMK2 cells were stained with an anti-Myc tag IgG primary antibody and an Alexa Fluor 488–conjugated goat anti-mouse IgG secondary antibody. The cells were mounted in VECTASHIELD mounting medium (Vector Laboratories) and imaged with a confocal laser

Published OnlineFirst December 18, 2012; DOI: 10.1158/1078-0432.CCR-12-1947

microscope (Radiance 2100; Bio-Rad Japan) equipped with the Laser Sharp 2000 software program.

Preparation of splenocytes

Spleens were isolated from female C57BL/6N mice, and the cells derived from the spleens were filtered through a 40-μm mesh sieve. These cells were hemolyzed with hemolysis buffer (Immno-Biological Laboratories Co., Ltd.), and the splenocytes were isolated.

In vitro measurement of IFN-γ

Splenocytes (2×10^5 cells/100 μL/well) were seeded on 96-well plates. scIL-12 or ZZ-scIL-12 (10, 20, or 2,000 pg) and HVJ-E [1.5 or 3×10^7 particles (F_1/F_2: fusion competent wild-type, F_0: fusion-incompetent wild-type, and ΔHN: HN-deleted type)] were added to the splenocytes in each experiment in a total volume of 100 μL of culture medium. The culture medium was collected 24 hours after treatment. The IFN-γ concentration of the culture medium was measured using an IFN-γ ELISA (R&D Systems, Inc.).

In vivo tumor volume measurement and depletion of CD4, CD8, and NK cells

Viable F10 melanoma cells (5×10^5 cells) were resuspended in 50 μL PBS and intradermally injected into the backs of female C57BL/6N mice. When each tumor had grown to 3 to 5 mm in diameter, the mice were treated with an intratumoral injection of wt-HVJ-E, scIL-12–HVJ-E (3×10^8 particles in a total volume of 100 μL), or 100 μL PBS on days 5, 7, and 9. Tumor volume was measured in a blind manner with slide calipers using the following formula: tumor volume (mm^3) = length × $(\text{width})^2/2$.

Anti-CD4 (clone GK1.5) and anti-CD8 (clone 53-7.62) antibodies were kindly provided by Dr. Murakami (Osaka University, Suita, Japan), and the anti-asialo GM1 antibody was purchased from Wako Pure Chemical Industries, Ltd.. To deplete the $CD4^+$ T cells, $CD8^+$ T cells, or NK cells, each antibody [anti-CD4 (200 μg), anti-CD8 (500 μg), and anti-asialo GM1 (20 μg)] was administered intraperitoneally on days 4, 5, 6, 7, 9, and 11, and the anti-asialo GM1 antibody (40 μg) was also administered intratumorally at the time of the scIL-12–HVJ-E administration. Rat IgG (Sigma) was used as a control for the anti-CD4 and anti-CD8 antibodies, and rabbit IgG (R&D Systems) was used as a control for the anti-asialo GM1 antibody.

Labeling of scIL-12–HVJ-E with ^{125}I

HVJ-E (wt-HVJ-E or scIL-12–HVJ-E) was labeled with iodine-125 radionuclide (^{125}I; PerkinElmer) using lactoperoxidase, and the ^{125}I-labeled HVJ-E was suspended in saline to a concentration of 6×10^8 particles/200 μL. The ^{125}I-labeled HVJ-E (200 μL) was intravenously injected into the tail veins of the mice, and tissues (brain, lungs, heart, liver, kidneys, spleen, muscle, and blood) were harvested from the mice after 24 hours. The ^{125}I level in the tissues was measured using γ-scintillation counting.

Systemic administration of scIL-12–HVJ-E

A viable F10 melanoma cell suspension (5×10^5 cells/200 μL PBS) was intravenously injected into the tail veins of female C57BL/6N mice followed by an injection of 300 μL PBS to avoid embolization of the vessels by the F10 melanomas. Beginning 5 days after the F10 melanoma injection, the mice received 3 intravenous injections of wt-HVJ-E, scIL-12–HVJ-E (6×10^8 particles/200 μL PBS), ZZ-scIL-12 (500 pg/200 μL PBS), or 200 μL PBS via the tail vein every other day. On day 14, the lungs were isolated from the mice after the last injection was administered, and the number of metastatic foci was counted.

^{51}Cr release CTL assays and ELISpot assays

wt-HVJ-E, scIL-12–HVJ-E, ZZ-scIL-12, or PBS was injected locally into the intradermal tumor masses or systemically via the tail vein in the mice bearing pulmonary metastases. The spleens were isolated from the mice 10 days after the last injection was administered. Splenocytes were isolated from the spleens as described earlier. F10 melanoma cells were treated with mitomycin C (15 μg/mL) for 45 minutes.

For the ^{51}Cr release CTL assays, the splenocytes and mitomycin C-treated F10 melanoma cells were mixed at a 10:1 ratio and cultured with culture medium that included 10 ng/mL recombinant mouse IL-2 (R&D Systems). Four days later, culture medium containing 5 ng/mL recombinant mouse IL-2 was added to the cultured cells, and the cells were cultured for another 3 days. Nonadherent splenocytes were collected, and serial 2-fold dilutions of splenocytes (20, 10, 5, 2.5, 1.25, and 0.625×10^5/100 μL/well) were made in 96-well plates. As positive and negative controls, 1% NP-40 and culture medium were added to the wells, respectively. The F10 melanoma cells were treated with the chromium-51 radionuclide (^{51}Cr; PerkinElmer Japan Co., Ltd.; 1.85 MBq/250 μL) for 45 minutes at 37°C and washed 3 times with RPMI-1640. A ^{51}Cr-labeled F10 melanoma suspension (2×10^4 cells/100 μL) was added to each well of the 96-well plate, which contained a 2-fold dilution of splenocytes, and the cells were incubated for 4 hours at 37°C. The supernatant of each well was collected after incubation, and the amount of ^{51}Cr released from the labeled F10 melanoma cells was determined using γ-scintillation counting.

For the ELISpot assay, the splenocytes and mitomycin C-treated F10 melanoma cells were mixed at a ratio of 10:1. Forty-eight hours later, nonadherent splenocytes were collected, and the ELISpot assay was conducted using the Mouse IFN-γ Development Module (R&D Systems) and the ELISpot Blue Color Module (R&D Systems). The number of IFN-γ–secreting cells was subsequently counted.

Real-time RT-PCR

On day 5 after the intravenous injection of the F10 melanoma cells, wt-HVJ-E, scIL-12–HVJ-E (6×10^8 particles/200 μL PBS), ZZ-scIL-12 (500 pg/200 μL PBS), or 200 μL PBS was intravenously injected into the tail veins of the mice once a day for 3 consecutive days. The lungs were isolated from the mice 24 hours after the last injection was

Published OnlineFirst December 18, 2012; DOI: 10.1158/1078-0432.CCR-12-1947

administered and homogenized in lysis buffer from the RNeasy Mini Kit (Invitrogen) using the Multi-Beads Shocker cell disruption system (Yasui Kikai Co.). Total RNA was isolated from the homogenized lung specimens using the RNeasy Mini Kit, and cDNA was synthesized from the RNA using High-Capacity cDNA Reverse Transcription Kits (Applied Biosystems Japan, Ltd.). IFN-γ and NKG2D mRNA were quantified with real-time reverse transcriptase PCR (RT-PCR) using the Real-time PCR Master Mix (Toyobo Co., Ltd.) and TaqMan Probes (Applied Biosystems Japan, Ltd.) for murine IFN-γ and NKG2D. In the same manner, glyceraldehyde-3-phosphate dehydrogenase (GAPDH) mRNA was quantified as a control.

Statistical analysis

The statistical analyses were conducted using the Tukey–Kramer test or Student unpaired *t* test, and *P* less than 0.05 was considered to be statistically significant.

Results

The HVJ-E F protein enhanced the IL-12–induced IFN-γ secretion in a fusion-independent manner

We have described the construction of the murine scIL-12 expression vector in a previous report (28). In this study, we used this vector to produce scIL-12 proteins in CHO cells. Stimulation of splenocytes from normal C57BL/6N mice with HVJ-E or scIL-12 (0.1 ng/mL) induced only a low level of IFN-γ secretion. However, we showed that the combining HVJ-E and scIL-12 dramatically enhanced the secretion of IFN-γ by the splenocytes (Fig. 1A). In addition, administration of a high dose of scIL-12 (10 ng/mL) induced IFN-γ secretion, but scIL-12 was significantly less effective than combined treatment with scIL-12 and HVJ-E (Fig. 1A). Next, we investigated which cells of the heterogeneous splenocyte population produced IFN-γ in response to scIL-12 and HVJ-E and found that IFN-γ was mainly produced by $CD3^+$ T cells (Supplementary Fig. S1).

The envelope of HVJ-E is composed of 2 different membrane proteins, the fusion protein (F) and HN. F exists in either the inactive F_0 form on fusion-incompetent HVJ-E or the enzymatically cleaved, active F_1/F_2 form on fusion-competent HVJ-E (33). Splenocytes were thus treated with either F_0- or F_1/F_2-HVJ-E in combination with scIL-12, and both types of HVJ-E induced robust IFN-γ secretion (Fig. 1B). Therefore, the HVJ-E–mediated enhancement of IFN-γ secretion was observed to be independent of fusion competence. Next, we investigated which membrane glycoproteins, HN or F, were responsible for the enhanced IFN-γ production. When administered with scIL-12, HN-depleted HVJ-E (ΔHN-HVJ-E), which displays increased F expression on the envelope, enhanced IFN-γ secretion more potently than wild-type HVJ-E (wt-HVJ-E; Fig. 1C), suggesting that F, but not HN, may be involved in the induction of IFN-γ production. Although both the F and HN proteins are present on the surface of the HVJ-E particle, the F protein is predominant. To generate F-depleted HVJ-E, the F protein of ΔHN-HVJ-E was enzymatically degraded by trypsin overtreatment (2.5 mg/mL for 24 hours at 37°C). F-depleted ΔHN-HVJ-E induced a significantly reduced level of IFN-γ secretion (Fig. 1D), and moreover, the anti-F antibody

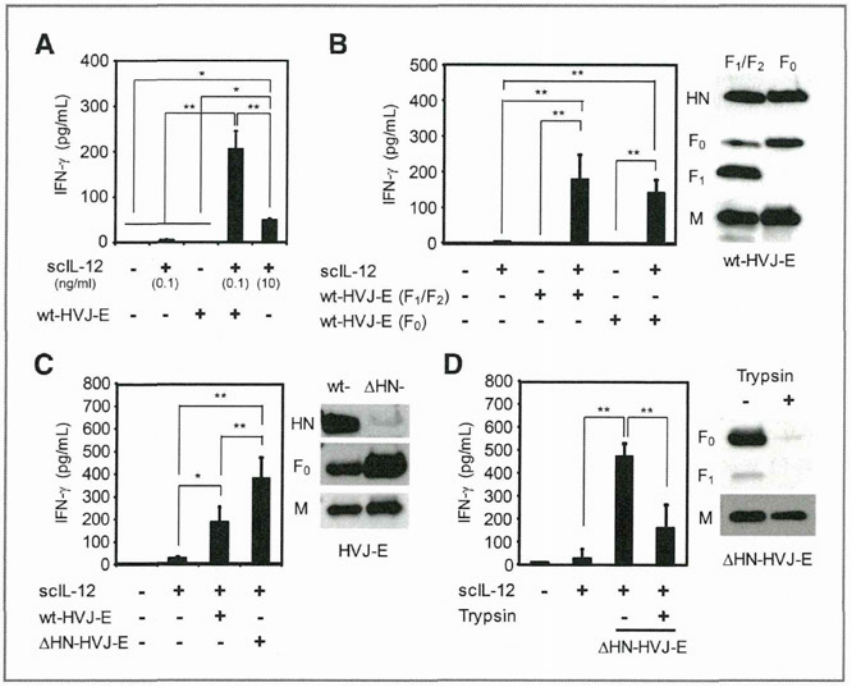

Figure 1. The synergistic effect of HVJ-E on IL-12–induced IFN-γ secretion. A–D, scIL-12 and/or various types of HVJ-E [(A) wt-HVJ-E (F_1/F_2), (B) F_1/F_2 or F_0 wt-HVJ-E, (C) wt-HVJ-E or ΔHN-HVJ-E, and (D) ΔHN-HVJ-E or F-degraded ΔHN-HVJ-E] were added to splenocytes, and 24 hours later, the IFN-γ concentrations of the supernatants were measured by ELISA. To confirm the protein composition of various types of HVJ-E, several viral proteins (HN, F_0, F_1, and M) were detected by Western blot analysis: (B) F_1/F_2 and F_0 wt-HVJ-E, (C) wt-HVJ-E and ΔHN-HVJ-E, and (D) ΔHN-HVJ-E and F-degraded ΔHN-HVJ-E. All data are presented as the mean ± SD ($n = 4$). *, $P < 0.05$; **, $P < 0.01$; Tukey–Kramer test.

Published OnlineFirst December 18, 2012; DOI: 10.1158/1078-0432.CCR-12-1947

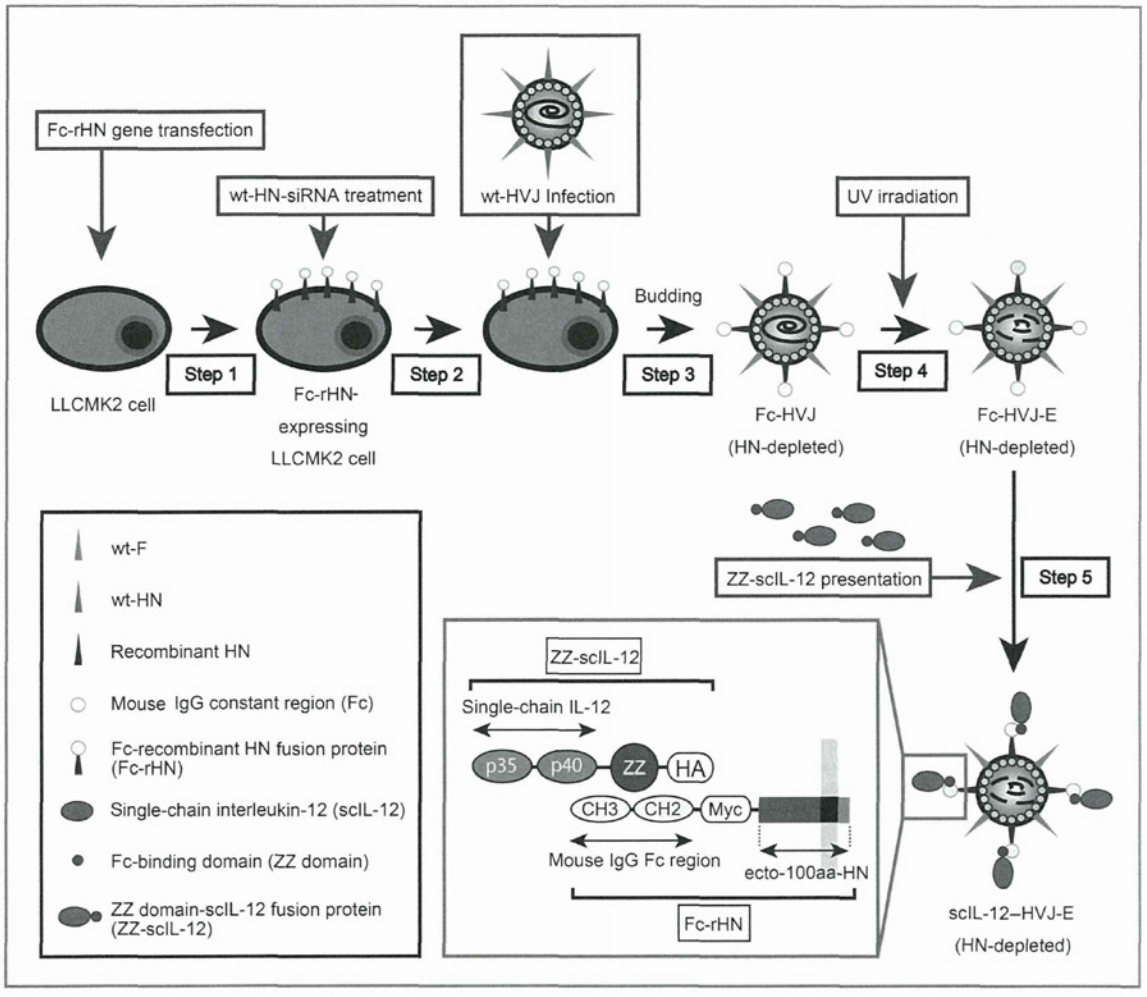

Figure 2. The construction of scIL-12–HVJ-E. LLCMK2 cells stably expressing Fc-HN were transfected with HN-siRNA. In LLCMK2, cells infected with live wt-HVJ, Fc-HVJ (HN-depleted) was produced as a viral progeny. Fc-HVJ-E (HN-depleted) was obtained after UV irradiation of the progeny. scIL-12–HVJ-E (HN-depleted) was constructed by conjugating ZZ-scIL-12 and Fc-HVJ-E (HN-depleted).

inhibited the induction of IFN-γ (Supplementary Fig. S2A), suggesting that the activity of the F protein is required for IFN-γ induction.

Overall strategy for the presentation of IL-12 on the surface of HVJ-E

These results prompted us to hypothesize that a close association between HVJ-E and IL-12 in the tumor microenvironment *in vivo* may synergistically enhance antitumor immunity. To prove this hypothesis, we generated scIL-12–conjugated HVJ-E (scIL-12–HVJ-E) that presents scIL-12 on the surface of ΔHN-HVJ-E by binding to the IgG constant region (Fc) and the protein A-Fc binding domain (ZZ; ref. 34) using viral gene engineering technology (35–37). This technology allowed for the manipulation of the HVJ-E membrane proteins by inducing the expression of recombinant envelope proteins on HVJ-infected cells (Fig. 2).

Generation of Fc-rHN and Fc-HVJ-E

To generate scIL-12–HVJ-E, we aimed to localize Fc-HN fusion proteins on the surface of ΔHN-HVJ-E. We constructed expression plasmids of HN deletion mutants (full length-, ecto-400aa-, ecto-300aa-, ecto-200aa-, and ecto-100aa-HN; Fig. 3A). Although all rHN proteins were expressed in the LLC-MK2 cells transfected with these plasmids (Fig. 3B), only ecto-100aa-HN was incorporated into the cell-derived progeny of HVJ by infecting rHN-expressing cells with live HVJ (Fig. 3C). Therefore, we constructed Fc-rHN, in which murine Fc was fused to the C-terminus of ecto-100aa-HN (Fig. 3D). We confirmed that Fc-rHN had the ability to bind to protein A using a coprecipitation assay with protein

Published OnlineFirst December 18, 2012; DOI: 10.1158/1078-0432.CCR-12-1947

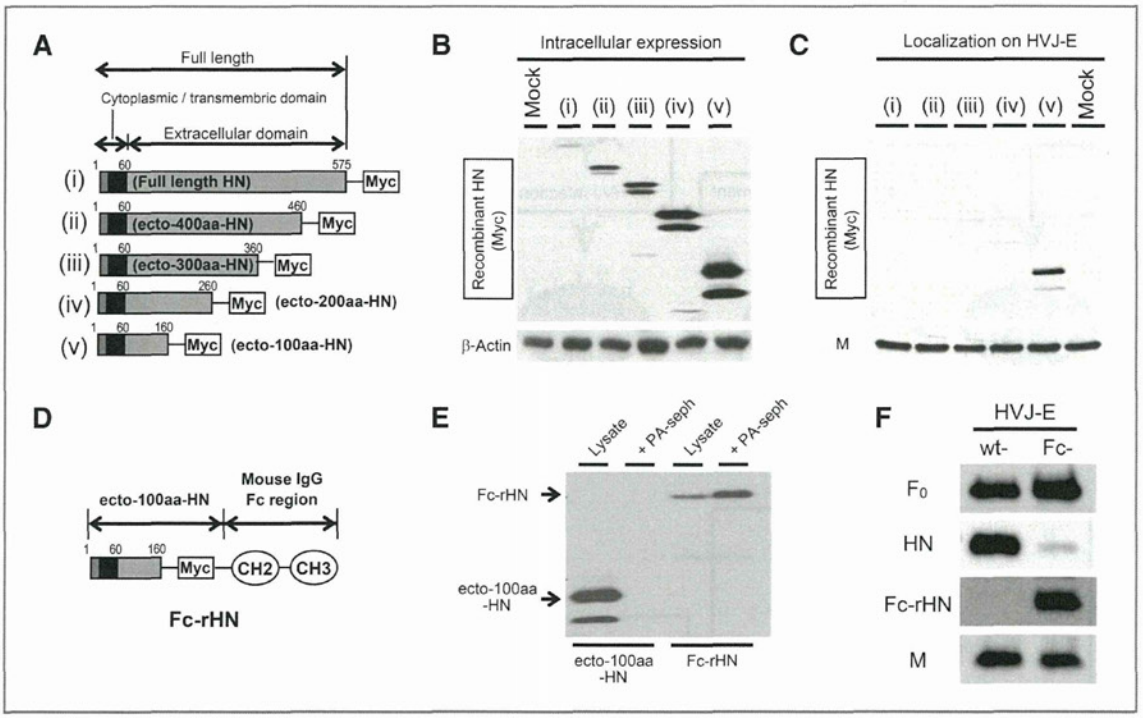

Figure 3. The construction of Fc-rHN and the generation of Fc-HVJ-E. A, the design of the recombinant deletion mutants of HN. (i) Full length-, (ii) ecto-400aa-, (iii) ecto-300aa-, (iv) ecto-200aa-, and (v) ecto-100aa-HN. B, the various *rHN* genes were transferred to LLC-MK2 cells, and their intracellular expression was detected using Western blot analysis. C, HVJ was used to infect rHN-expressing LLC-MK2 cells, and the rHN in the cell-derived HVJ-E progeny was detected using Western blot analysis. D, Fc-rHN, (E) Fc-rHN or ecto-100aa-HN was mixed with protein A-Sepharose, and the rHN that coprecipitated with protein A-Sepharose (PA-seph) was detected using Western blot analysis. F, the expression of the viral proteins (HN, F, M, and Fc-rHN) of Fc-HVJ-E and wt-HVJ-E was examined using Western blot analysis.

A-Sepharose (Fig. 3E). We then generated Fc-HVJ-E, which included Fc-rHN with depleted wt-HN (Fig. 3F).

Generation of ZZ-scIL-12 and scIL-12–HVJ-E

To present scIL-12 on the surface of Fc-HVJ-E, we constructed ZZ-scIL-12 by inserting the ZZ domain into the downstream scIL-12 signal peptide (Fig. 4A). ZZ-scIL-12 and scIL-12 induced IFN-γ secretion by splenocytes (Fig. 4A). Next, we investigated the ability of ZZ-scIL-12 to bind to Fc-rHN on Fc-HVJ-E using sucrose density gradient centrifugation. When analyzed separately, ZZ-scIL-12 was detected in the upper layer, and HVJ-E was detected in the lower layer of the 25% to 50% sucrose gradients (Supplementary Fig. S3). However, ZZ-scIL-12 was shifted to the lower layer in the sedimentation of the ZZ-scIL-12 and Fc-HVJ-E mixture (Fig. 4B), suggesting that ZZ-scIL-12 binds to Fc-rHN on Fc-HVJ-E. Moreover, ZZ-scIL-12–conjugated Fc-HVJ-E (scIL-12–HVJ-E) was incubated in murine serum, and ZZ-scIL-12 was maintained in Fc-HVJ-E for 24 hours (Fig. 4C). We calculated the amount of ZZ-scIL-12 on Fc-HVJ-E by comparing the density of the bands corresponding to ZZ-scIL-12 by Western blot analysis and estimated that approximately 6.83 molecules of ZZ-scIL-12 were loaded onto 1 particle of Fc-HVJ-E (Supplementary Fig. S4). Finally, scIL-12–HVJ-E displayed much stronger IFN-γ–inducing activity on splenocytes and dendritic cells than wt-HVJ-E or scIL-12 alone (Fig. 4D and Supplementary Fig. S2B).

Antitumor effects against intradermal F10 melanomas induced by the intratumoral administration of scIL-12–HVJ-E

We next investigated the antitumor activity of scIL-12–HVJ-E *in vivo*. A murine intradermal tumor model was generated through intradermal inoculation of F10 melanoma cells (5×10^5 cells) into the backs of female C57BL/6N mice. When each tumor had grown to approximately 3 to 5 mm in diameter, scIL-12–HVJ-E, wt-HVJ-E, or PBS was injected into the tumor for a total of 3 times every other day. In these experiments, scIL-12–HVJ-E caused a much more robust tumor suppression than wt-HVJ-E (Fig. 5A). Moreover, the antitumor immune responses against the F10 melanomas were examined using ^{51}Cr release CTL assays (Fig. 5B) and ELISpot assays (Fig. 5C). The data revealed that scIL-12–HVJ-E remarkably enhanced CTL activity against F10 melanomas. Next, to investigate the roles of $CD4^+$ T cells, $CD8^+$ T cells, and NK cells in the therapeutic effect, scIL-12–HVJ-E–mediated tumor growth inhibition was assessed in mice depleted of $CD4^+$ T cells, $CD8^+$ T cells,

Published OnlineFirst December 18, 2012; DOI: 10.1158/1078-0432.CCR-12-1947

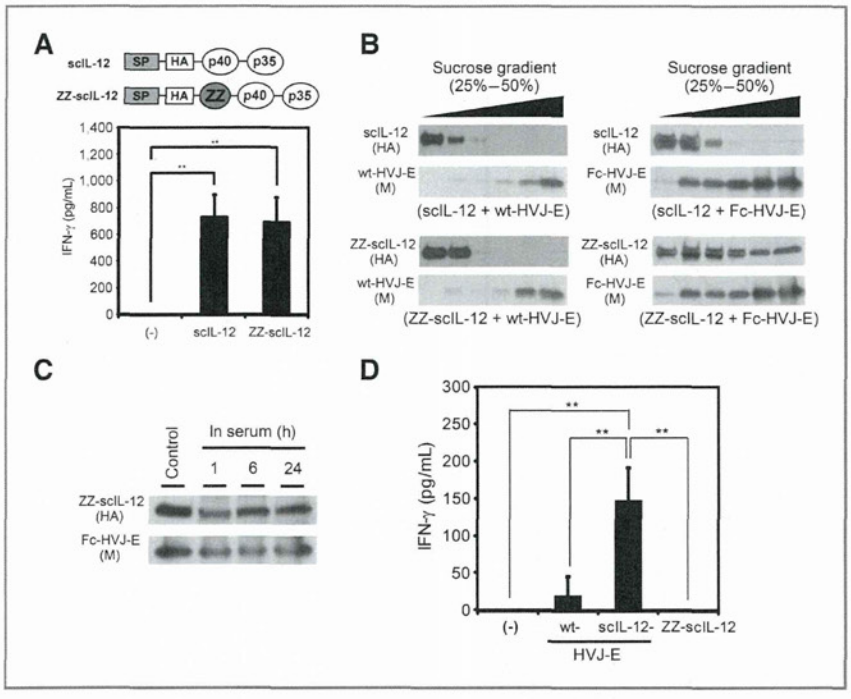

Figure 4. The construction of ZZ-scIL-12 and the generation of scIL-12–HVJ-E. A, splenocytes were incubated with 10 ng/mL scIL-12 or ZZ-scIL-12 (2 ng/100 μL for each) for 48 hours, and the IFN-γ concentrations of the supernatants were measured by ELISA. B, scIL-12 or ZZ-scIL-12 was mixed with wt-HVJ-E or Fc-HVJ-E, and each mixture was treated to fractionation by 25% to 50% sucrose gradient. The scIL-12 or ZZ-scIL-12 and wt-HVJ-E or Fc-HVJ-E in each fraction was detected using Western blot analysis. An anti-HA antibody was used to detect scIL-12 and ZZ-scIL-12, and an anti-M antibody was used to detect wt-HVJ-E and Fc-HVJ-E. C, Fc-HVJ-E bound with ZZ-scIL-12 was incubated in murine serum at 37°C for 1, 6, or 24 hours and then subjected to sucrose gradient centrifugation. After isolating the Fc-HVJ-E fraction, ZZ-scIL-12 and Fc-HVJ-E were detected using Western blot analysis. D, wt-HVJ-E, scIL-12–HVJ-E (1.5×10^7 particles), or ZZ-scIL-12 (12.5 pg) in 100 μL PBS was added to the splenocytes for 24 hours, and the IFN-γ concentrations of the supernatants were measured by ELISA. All data are presented as the mean ± SD ($n = 4$). **, $P < 0.01$; Tukey–Kramer test.

and NK cells by administrating a neutralizing antibody specific for each cell type (13, 38). The depletion of CD8 and NK cells, but not CD4 cells, significantly decreased the scIL-12–HVJ-E–mediated effect (Fig. 5D–F), showing that the antitumor effect of scIL-12–HVJ-E was dependent on $CD8^+$ T cells and NK cells but not $CD4^+$ T cells.

Antitumor effects against metastatic lung F10 melanomas induced by the systemic administration of scIL-12–HVJ-E

We then investigated the tissue distribution of scIL-12–HVJ-E following intravenous injection. ^{125}I-labeled HVJ-E was systemically administered via tail vein injection, and the level of ^{125}I in the tissues (brain, lungs, heart, liver, kidneys, spleen, muscles, and blood) was measured using a γ-scintillation counter 24 hours after injection. Interestingly, scIL-12–HVJ-E and ΔHN-HVJ-E, but not wt-HVJ-E, preferentially accumulated in the lungs (Fig. 6A and Supplementary Fig. S5A), implying that HN depletion likely affected the localization of HVJ-E.

We next investigated the therapeutic effects of intravenous scIL-12–HVJ-E administration in a murine F10 melanoma model of lung metastasis. The mice were inoculated with F10 melanoma cells (5×10^5 cells) by intravenous injection. Multiple metastatic foci appeared on the surface of the lungs 5 days after the F10 melanoma injection (Supplementary Fig. S5B). We began intravenous administration of scIL-12–HVJ-E, wt-HVJ-E, or ZZ-scIL-12 when lung metastasis was confirmed. The injections were repeated for a total of 3 times every other day. As expected, only the scIL-12–HVJ-E–treated mice exhibited a significant reduction in the number of metastatic foci in the lungs (Fig. 6B). On the basis of our microarray analysis of the lung transcripts (data not shown), we focused on IFN-γ and NKG2D, which showed increased expression upon scIL-12–HVJ-E treatment. Real-time RT-PCR analysis confirmed that IFN-γ and NKG2D expression were both increased in lungs treated with scIL-12–HVJ-E (Fig. 6C). Although IFN-γ expression was found to be elevated in the lungs, the serum IFN-γ level was unchanged by scIL-12–HVJ-E administration (Supplementary Fig. S6A). However, the coadministration of scIL-12 and Fc-HVJ-E increased the serum IFN-γ level (Supplementary Fig. S6B). Moreover, scIL-12–HVJ-E significantly induced NKG2D expression in the lungs, suggesting that NK cells and $CD8^+$ T lymphocytes were activated in the lesions (Fig. 6C). Systemic administration of scIL-12–HVJ-E

Published OnlineFirst December 18, 2012; DOI: 10.1158/1078-0432.CCR-12-1947

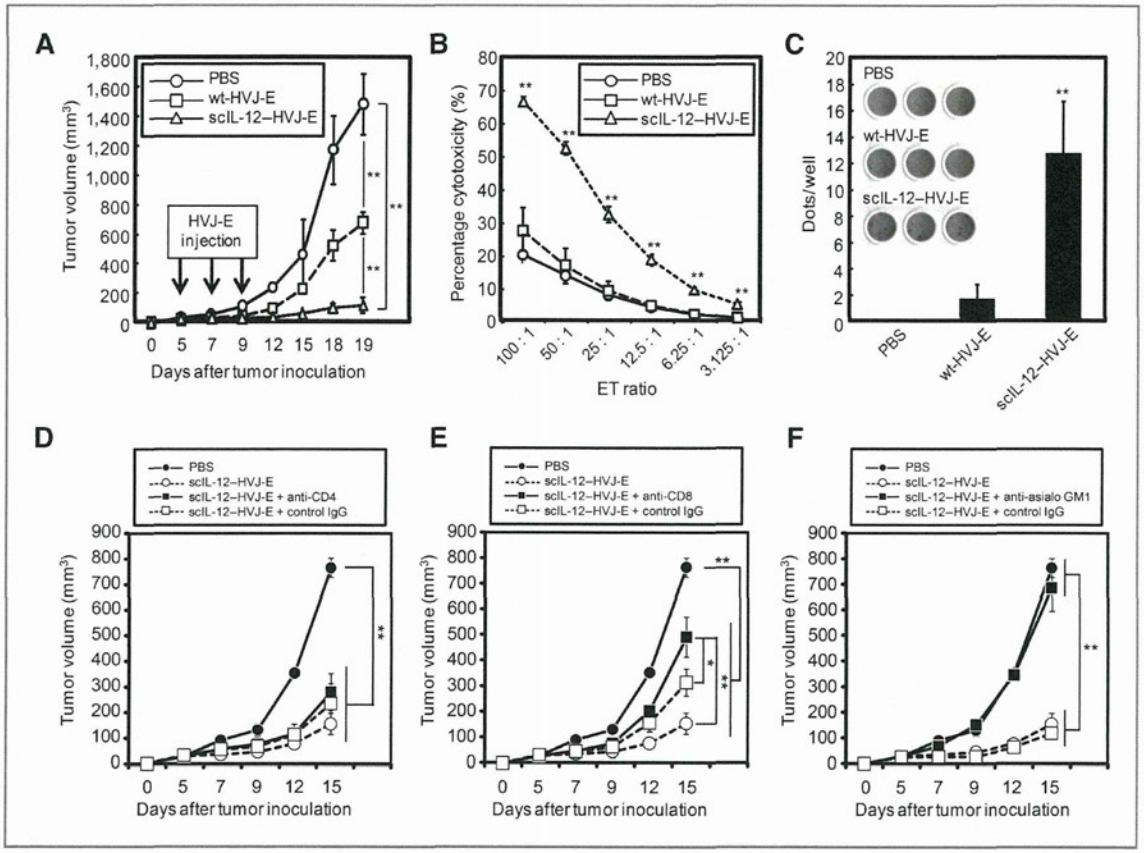

Figure 5. The antitumor effects induced by the intratumoral administration of scIL-12–HVJ-E. F10 melanoma cells (5×10^5 cells) were inoculated into the intradermal spaces in the backs of mice (day 0), and wt-HVJ-E, scIL-12–HVJ-E, or PBS was intratumorally administered on days 5, 7, and 9. A, tumor volume was assessed daily. B, the CTL activity against the F10 melanomas was measured using a ^{51}Cr release assay. C, F10 melanoma-specific IFN-γ secretion from splenocytes was measured using an ELISpot assay. D–F, F10 melanoma-bearing mice were generated by inoculating the tumor cells into their backs (day 0). PBS or scIL-12–HVJ-E was intratumorally administered on days 5, 7, and 9, and tumor volume was assessed daily. For the depletion of $CD4^+$ (D) or $CD8^+$ (E) T cells, anti-CD4 (200 μg) or anti-CD8 (500 μg) antibodies were intraperitoneally administered on days 4, 5, 6, 7, 9, and 11. For the depletion of NK cells (F), the anti-asialo GM1 antibody was administered intraperitoneally (20 μg) on days 4, 5, 6, 7, 9, and 11 and intratumorally (40 μg) on days 5, 7, and 9. All data are presented as the mean ± SD ($n = 3$). *, $P < 0.05$; **, $P < 0.01$; Tukey–Kramer test.

induced robust activation of CTLs specific for melanoma (Fig. 6D), and no evident adverse effects were observed in the treated mice. The CTL activation was significantly reduced by an anti-IFN-γ antibody, indicating that the CTL activation was dependent on IFN-γ (Supplementary Fig. S7A). Moreover, the CTLs targeted melanoma cells specifically, as the cytotoxic effects were not detected in other cells (Supplementary Fig. S7B).

Discussion

In this study, we showed that HVJ-E dramatically enhances IL-12 activity and induces IFN-γ production in splenocytes. The systemic administration of IL-12–conjugated HVJ-E significantly increases the level of IFN-γ expression in the lungs without elevating the serum IFN-γ level and effectively induces antitumor activity against metastatic lung melanomas.

Previously, our group reported that several components of HVJ-E stimulate tumor cells and dendritic cells to secrete various cytokines. RNA genome fragments of HVJ-E, which are taken into host cells through membrane fusion, are recognized by RIG-I but not TLRs (39), and type-I IFN is induced in tumor cells and dendritic cells. However, F_0-formed HVJ-E, which is unable to fuse with host cells, enhances scIL-12–induced IFN-γ secretion (Fig. 1B). Therefore, the activation of RIG-I by RNA fragments is unlikely to be correlated with IFN-γ enhancement. In this study, we showed that F is responsible for enhancing IFN-γ secretion (Fig. 1C and D). Although our previous report shows that F induces IL-6 secretion in dendritic cells in a fusion-independent manner (40), F-mediated IL-6 secretion does not mediate IFN-γ enhancement because IL-6 does not enhance IL-12 activity (41, 42). These results suggest that putative F receptors on

Published OnlineFirst December 18, 2012; DOI: 10.1158/1078-0432.CCR-12-1947

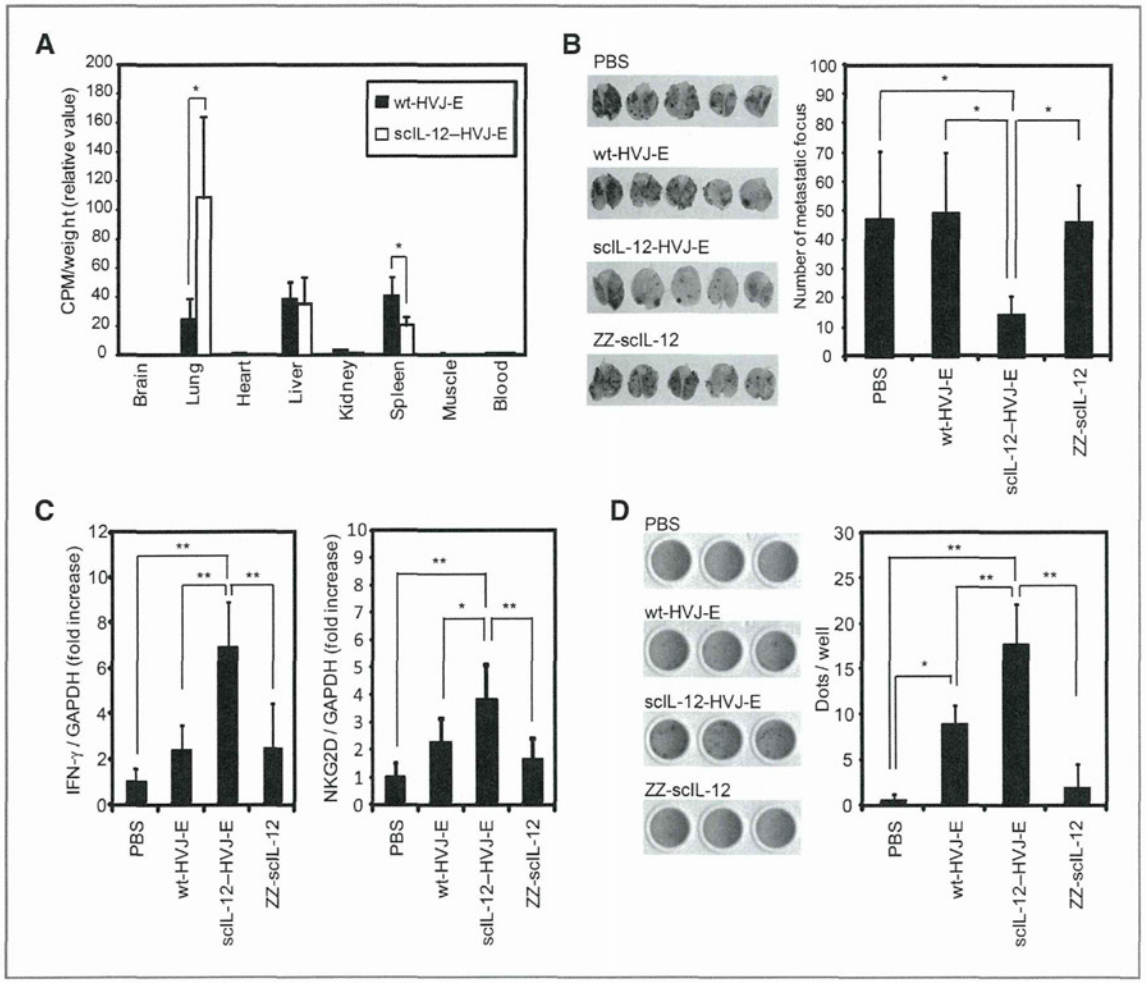

Figure 6. Treatment of lung metastatic F10 melanomas with systemically administered scIL-12–HVJ-E. A, ^{125}I-labeled wt-HVJ-E or scIL-12–HVJ-E was injected into the murine tail vein, and 24 hours later, the ^{125}I level in various tissues (brain, lungs, heart, liver, kidneys, spleen, muscles, and blood) was measured using a γ-scintillation counter ($n = 5$). B–D, wt-HVJ-E, scIL-12–HVJ-E, ZZ-scIL-12, or PBS was systemically administered 3 times into the tail veins of mice bearing metastatic F10 lung melanomas. B, the lungs were isolated, and the number of pulmonary metastatic foci was counted ($n = 5$). C, the expression levels of IFN-γ and NKG2D in the lungs were measured using real-time RT-PCR ($n = 4$). D, the level of F10 melanoma-specific IFN-γ secretion by splenocytes was assessed using an ELISpot assay (PBS and ZZ-scIL-12, $n = 3$; wt-HVJ-E and scIL-12–HVJ-E, $n = 4$). All data are presented as the mean ± SD. *, $P < 0.05$; **, $P < 0.01$; Tukey–Kramer test.

splenocytes may transmit signals to enhance IFN-γ and IL-12 production.

ΔHN-HVJ-E enhanced IFN-γ induction more robustly than wt-HVJ-E because the expression levels of F in ΔHN-HVJ-E were increased by knocking down HN (37 and Fig. 1C). Because HN induces hemagglutination by binding to sialic acid on the surface receptors of red blood cells (43), the administration of wt-HVJ-E, especially intravenously, has limitations for cancer therapy. ΔHN-HVJ-E shows very low hemagglutinating activity (37) and robustly enhances IFN-γ and IL-12 production *in vitro*.

In the experiments shown in Fig. 5D–F, although CD8$^+$ T cells and NK cells were required for scIL-12–HVJ-E–mediated antitumor effects, the depletion of CD4$^+$ T cells did not affect the suppression of tumor growth by scIL-12–HVJ-E. Previous reports have indicated that the IL-12–mediated antitumor response is maintained in CD4$^+$ T-cell–depleted mice (44) and that IL-12 stimulates antigen-specific CD8$^+$ T cells in CD4$^+$ T-cell knockout mice (45). Therefore, we suggest that scIL-12–HVJ-E–mediated antitumor immunity was independent of CD4$^+$ T cells. Moreover, in Fig. 5D–F and Supplementary Fig. S7, the peritoneal administration of a large amount of control IgG (more than 200 μg) induced a small decrease in scIL-12–HVJ-E–mediated antitumor immunity. Although the precise mechanism is unclear, this result might be due to the immunosuppressive

Published OnlineFirst December 18, 2012; DOI: 10.1158/1078-0432.CCR-12-1947

effect of the administration of a large amount of IgG (intravenous immunogloburin; ref. 46).

In previous reports, the Fc-ZZ–binding system has been applied to various types of targeting vectors (47–49), and we hypothesized that scIL-12–HVJ-E generated using this system could be functional upon systemic administration in mice. In fact, the Fc-ZZ binding of scIL-12–HVJ-E was stable in serum for at least 24 hours (Fig. 4C), and intravenous administration of scIL-12–HVJ-E resulted in elevated IFN-γ expression levels in the lungs due to pulmonary accumulation of the virions (Fig. 6A and C).

scIL-12–HVJ-E and ΔHN-HVJ-E, but not wt-HVJ-E, preferentially accumulated in the lungs (Fig. 6A and Supplementary Fig. S5A). A previous report has indicated that HVJ-E preferentially accumulates in spleen after intravenous administration (50). This accumulation in the spleen most likely occurs because HN on HVJ-E induces hemagglutination by binding to the sialic acid on the erythrocyte surface, causing the erythrocyte and HVJ-E complex to be transported to the spleen and degraded. Therefore, the accumulation of scIL-12–HVJ-E and ΔHN-HVJ-E in the lung may result from the loss of hemagglutinating activity upon HN knockdown and the subsequent escape from the "spleen-trap"; however, the precise mechanism by which this occurs remains unclear.

A previous study has shown that only high doses (~0.5–1.0 μg) of systemic IL-12 suppress tumor growth in mice by inducing a significant elevation in the serum IFN-γ level (30). However, such increases in serum IFN-γ have been shown to induce serious side effects, such as stomatitis, gastrointestinal bleeding, colitis, and diarrhea (31, 32). Therefore, the systemic administration of IL-12 has not been applied for clinical use thus far. We herein showed that systemically administered scIL-12–HVJ-E, which contains approximately 500 pg scIL-12, preferentially accumulated in the lungs (Fig. 6A) and mediated the synergistic antitumor effects of HVJ-E and IL-12 in the tumor microenvironment (Fig. 6B and C) without elevating the serum IFN-γ levels (Supplementary Fig. S6A). In contrast, the coadministration of scIL-12 and Fc-HVJ-E increased the serum IFN-γ level (Supplementary Fig. S6B). Therefore, the conjugation of IL-12 and HVJ-E is important to inhibit the elevation of serum IFN-γ, which may cause severe side effects (31, 32). The data shown here provide a basis for the future clinical application of scIL-12–HVJ-E, which seems to have a higher anticancer activity and lower toxicity than IL-12 alone.

Disclosure of Potential Conflicts of Interest

No potential conflicts of interest were disclosed.

Authors' Contributions

Conception and design: Y. Kaneda
Development of methodology: K. Saga, K. Tamai, Y. Kaneda
Acquisition of data (provided animals, acquired and managed patients, provided facilities, etc.): K. Saga
Analysis and interpretation of data (e.g., statistical analysis, biostatistics, computational analysis): K. Saga, K. Tamai, Y. Kaneda
Writing, review, and/or revision of the manuscript: K. Saga, Y. Kaneda
Administrative, technical, or material support (i.e., reporting or organizing data, constructing databases): K. Saga, T. Yamazaki, Y. Kaneda
Study supervision: K. Saga, Y. Kaneda

Grant Support

This work was supported by the Northern Osaka (Saito) Biomedical Knowledge-Based Cluster Creation Project, Special Coordination Funds for Promoting Science from the Ministry of Education, Culture, Sports, Science and Technology of Japan, and grants from the Ministry of Health, Labor and Welfare of Japan.

The costs of publication of this article were defrayed in part by the payment of page charges. This article must therefore be hereby marked *advertisement* in accordance with 18 U.S.C. Section 1734 solely to indicate this fact.

Received June 14, 2012; revised November 9, 2012; accepted November 19, 2012; published OnlineFirst December 18, 2012.

References

1. Vignali DAA, Collison LW, Workman CJ. How regulatory T cells work. Nat Rev Immunol 2008;8:523–32.
2. Burch PA, Croghan GA, Gastineau DA, Jones LA, Kaur JS, Kylstra JW, et al. Immunotherapy (APC8015, Provenge®) targeting prostatic acid phosphatase can induce durable remission of metastatic androgen-independent prostate cancer: a phase 2 trial. Prostate 2004;60:197–204.
3. Cheever MA, Higano CS. PROVENGE (Sipuleucel-T) in prostate cancer: the first FDA-approved therapeutic cancer vaccine. Clin Cancer Res 2011;17:3520–6.
4. Hodi FS, O'Day SJ, McDermott DF, Weber RW, Sosman JA, Haanen JB, et al. Improved survival with ipilimumab in patients with metastatic melanoma. N Engl J Med 2010;363:711–23.
5. Prieto PA, Yang JC, Sherry RM, Hughes MS, Kammula US, White DE, et al. CTLA-4 blockade with ipilimumab: long-term follow-up of 177 patients with metastatic melanoma. Clin Cancer Res 2012;18:2039–47.
6. Topalian SL, Hodi FS, Brahmer JR, Gettinger SN, Smith DC, McDermott DF, et al. Safety, activity, and immune correlates of anti–PD-1 antibody in cancer. N Engl J Med 2012;366:2443–54.
7. Dudley ME, Yang JC, Sherry R, Hughes MS, Royal R, Kammula U, et al. Adoptive cell therapy for patients with metastatic melanoma: evaluation of intensive myeloablative chemoradiation preparative regimens. J Clin Oncol 2008;26:5233–9.
8. Kirkwood JM, Tarhini AA, Panelli MC, Moschos SJ, Zarour HM, Butterfield LH, et al. Next generation of immunotherapy for melanoma. J Clin Oncol 2008;26:3445–55.
9. Mellman I, Coukos G, Dranoff G. Cancer immunotherapy comes of age. Nature 2011;480:480–9.
10. Lamb RA, Kolakofsky D. Paramyxoviridae: the viruses and their replicaiton. Fields Virol 2001:1305–40.
11. Curran J, Kolakofsky D. Replication of paramyxoviruses. Adv Virus Res 1999;54:403–22.
12. Kurooka M, Kaneda Y. Inactivated Sendai virus particles eradicate tumors by inducing immune responses through blocking regulatory T cells. Cancer Res 2007;67:227–36.
13. Fujihara A, Kurooka M, Miki T, Kaneda Y. Intratumoral injection of inactivated Sendai virus particles elicits strong antitumor activity by enhancing local CXCL10 expression and systemic NK cell activation. Cancer Immunol Immunother 2008;57:73–84.
14. Pasare C, Medzhitov R. Toll pathway-dependent blockade of $CD4^+$ $CD25^+$ T cell-mediated suppression by dendritic cells. Science 2003;299:1033–6.
15. Lal G, Zhang N, Van Der Touw W, Ding Y, Ju W, Bottinger EP, et al. Epigenetic regulation of Foxp3 expression in regulatory T cells by DNA methylation. J Immunol 2009;182:259–73.
16. Benveniste EN. Cytokine actions in the central nervous system. Cytokine Growth Factor Rev 1998;9:259–75.

Published OnlineFirst December 18, 2012; DOI: 10.1158/1078-0432.CCR-12-1947

17. Tannenbaum CS, Tubbs R, Armstrong D, Finke JH, Bukowski RM, Hamilton TA. The CXC chemokines IP-10 and Mig are necessary for IL-12-mediated regression of the mouse RENCA tumor. J Immunol 1998;161:927–32.
18. Bukowski RM, Rayman P, Molto L, Tannenbaum CS, Olencki T, Peereboom D, et al. Interferon-γ and CXC chemokine induction by interleukin 12 in renal cell carcinoma. Clin Cancer Res 1999;5:2780–9.
19. Seliger B, Hammers S, Höhne A, Zeidler R, Knuth A, Gerharz CD, et al. IFN-gamma-mediated coordinated transcriptional regulation of the human TAP-1 and LMP-2 genes in human renal cell carcinoma. Clin Cancer Res 1997;3:573–8.
20. Weber JS, Rosenberg SA. Modulation of murine tumor major histocompatibility antigens by cytokines *in vivo* and *in vitro*. Cancer Res 1988;48:5818–24.
21. Nakajima C, Uekusa Y, Iwasaki M, Yamaguchi N, Mukai T, Gao P, et al. A role of interferon-γ (IFN-γ) in tumor immunity T cells with the capacity to reject tumor cells are generated but fail to migrate to tumor sites in IFN-γ-deficient mice. Cancer Res 2001;61:3399–405.
22. Pujade-Lauraine E, Guastalla JP, Colombo N, Devillier P, François E, Fumoleau P, et al. Intraperitoneal recombinant interferon gamma in ovarian cancer patients with residual disease at second-look laparotomy. J Clin Oncol 1996;14:343–50.
23. Windbichler GH, Hausmaninger H, Stummvoll W, Graf AH, Kainz C, Lahodny J, et al. Interferon-gamma in the first-line therapy of ovarian cancer: a randomized phase III trial. Br J Cancer 2000;82:1138–44.
24. Giannopoulos A, Constantinides C, Fokaeas E, Stravodimos C, Giannopoulou M, Kyroudi A, et al. The immunomodulating effect of interferon-γ intravesical instillations in preventing bladder cancer recurrence. Clin Cancer Res 2003;9:5550–8.
25. Marth C, Windbichler GH, Hausmaninger H, Petru E, Estermann K, Pelzer A, et al. Interferon-gamma in combination with carboplatin and paclitaxel as a safe and effective first-line treatment option for advanced ovarian cancer: results of a phase I/II study. Int J Gynecol Cancer 2006;16:1522–8.
26. Colombo MP, Trinchieri G. Interleukin-12 in anti-tumor immunity and immunotherapy. Cytokine Growth Factor Rev 2002;13:155–68.
27. Watford WT, Moriguchi M, Morinobu A, O'Shea JJ. The biology of IL-12: coordinating innate and adaptive immune responses. Cytokine Growth Factor Rev 2003;14:361–8.
28. Lieschke GJ, Rao PK, Gately MK, Mulligan RC. Bioactive murine and human interleukin-12 fusion proteins which retain antitumor activity *in vivo*. Nat Biotechnol 1997;15:35–40.
29. Foss DL, Moody MD, Murphy KP Jr, Pazmany C, Zilliox MJ, Murtaugh MP. *In vitro* and *in vivo* bioactivity of single-chain interleukin-12. Scand J Immunol 1999;50:596–604.
30. Nastala CL, Edington HD, McKinney TG, Tahara H, Nalesnik MA, Brunda MJ, et al. Recombinant IL-12 administration induces tumor regression in association with IFN-gamma production. J Immunol 1994;153:1697–706.
31. Atkins MB, Robertson MJ, Gordon M, Lotze MT, DeCoste M, DuBois JS, et al. Phase I evaluation of intravenous recombinant human interleukin 12 in patients with advanced malignancies. Clin Cancer Res 1997;3:409–17.
32. Leonard JP, Sherman ML, Fisher GL, Buchanan LJ, Larsen G, Atkins MB, et al. Effects of single-dose interleukin-12 exposure on interleukin-12-associated toxicity and interferon-gamma production. Blood 1997;90:2541–8.
33. Tashiro M, McQueen NL, Seto JT. Determinants of organ tropism of Sendai virus. Front Biosci 1999;4:D642–45.
34. Nilsson B, Moks T, Jansson B, Abrahmsén L, Elmblad A, Holmgren E, et al. A synthetic IgG-binding domain based on staphylococcal protein A. Protein Eng 1987;1:107–13.
35. Kawachi M, Tamai K, Saga K, Yamazaki T, Fujita H, Shimbo T, et al. Development of tissue-targeting hemagglutinating virus of Japan envelope vector for successful delivery of therapeutic gene to mouse skin. Hum Gene Ther 2007;18:881–94.
36. Shimbo T, Kawachi M, Saga K, Fujita H, Yamazaki T, Tamai K, et al. Development of a transferrin receptor-targeting HVJ-E vector. Biochem Biophys Res Commun 2007;364:423–8.
37. Saga K, Tamai K, Kawachi M, Shimbo T, Fujita H, Yamazaki T, et al. Functional modification of Sendai virus by siRNA. J Biotechnol 2008; 133:386–94.
38. Lee J, Nakagiri T, Oto T, Harada M, Morii E, Shintani Y, et al. IL-6 amplifier, NF-κB–triggered positive feedback for IL-6 signaling, in grafts is involved in allogeneic rejection responses. J Immunol 2012; 189:1928–36.
39. López CB, Moltedo B, Alexopoulou L, Bonifaz L, Flavell RA, Moran TM. TLR-independent induction of dendritic cell maturation and adaptive immunity by negative-strand RNA viruses. J Immunol 2004;173: 6882–9.
40. Suzuki H, Kurooka M, Hiroaki Y, Fujiyoshi Y, Kaneda Y. Sendai virus F glycoprotein induces IL-6 production in dendritic cells in a fusion-independent manner. FEBS Lett 2008;582:1325–9.
41. Rincón M, Anguita J, Nakamura T, Fikrig E, Flavell RA. Interleukin (IL)-6 directs the differentiation of IL-4–producing CD4$^+$ T cells. J Exp Med 1997;185:461–70.
42. Frassanito MA, Cusmai A, Dammacco F. Deregulated cytokine network and defective Th1 immune response in multiple myeloma. Clin Exp Immunol 2001;125:190–7.
43. Portner A, Scroggs RA, Metzger DW. Distinct functions of antigenic sites of the HN glycoprotein of sendai virus. Virology 1987;158:61–8.
44. Brunda MJ, Luistro L, Warrier RR, Wright RB, Hubbard BR, Murphy M, et al. Antitumor and antimetastatic activity of interleukin 12 against murine tumors. J Exp Med 1993;178:1223–30.
45. Schmidt CS, Mescher MF. Peptide antigen priming of naive, but not memory, CD8 T cells requires a third signal that can be provided by IL-12. J Immunol 2002;168:5521–9.
46. Ephrem A, Chamat S, Miquel C, Fisson S, Mouthon L, Caligiuri G, et al. Expansion of CD4$^+$CD25$^+$ regulatory T cells by intravenous immunoglobulin: a critical factor in controlling experimental autoimmune encephalomyelitis. Blood 2008;111:715–22.
47. Morizono K, Bristol G, Xie Y, Kung SK-P, Chen ISY. Antibody-directed targeting of retroviral vectors via cell surface antigens. J Virol 2001;75:8016–20.
48. Henning P, Andersson KME, Frykholm K, Ali A, Magnusson MK, Nygren P-A, et al. Tumor cell targeted gene delivery by adenovirus 5 vectors carrying knobless fibers with antibody-binding domains. Gene Ther 2005;12:211–24.
49. Morizono K, Xie Y, Ringpis G-E, Johnson M, Nassanian H, Lee B, et al. Lentiviral vector retargeting to P-glycoprotein on metastatic melanoma through intravenous injection. Nat Med 2005;11:346–52.
50. Kaneda Y, Nakajima T, Nishikawa T, Yamamoto S, Ikegami H, Suzuki N, et al. Hemagglutinating virus of Japan (HVJ) envelope vector as a versatile gene delivery system. Mol Ther 2002;6:219–26.